Real-space mean-field approach to polymeric ternary systems

Shigeyuki Komura[a)]
Department of Chemistry, Faculty of Science, Tokyo Metropolitan University, Tokyo 192-0397, Japan

Hiroya Kodama[b)]
Science and Technology Research Center, Mitsubishi Chemical Corporation, Yokohama 227-8502, Japan

Keizo Tamura
Department of Chemistry, Faculty of Science, Tokyo Metropolitan University, Tokyo 192-0397, Japan

(Received 22 April 2002; accepted 4 September 2002)

Phase separated structure of ternary blends of A and B homopolymers and symmetric AB diblock copolymer is investigated using a lattice (real-space) self-consistent field theory. This paper includes the detailed description of our published results [Kodama, Komura, and Tamura, Europhys. Lett. **53**, 46 (2001)] as well as more extended calculations. We consider the symmetric case, namely, (i) both A and B homopolymers have the same degree of polymerization $N_A=N_B$; (ii) AB diblock copolymer of length N_{AB} is symmetric; (iii) average volume fractions of A and B homopolymers are equal. We looked into the influence of relative chain lengths $\alpha=N_A/N_{AB}$ on the phase separated structure. Our numerical simulations are performed in the real space *without* assuming the symmetry of the structure *a priori*. For the fixed copolymer length and $\alpha<1$, the typical length scale of the microphase separated structure become smaller for relatively shorter homopolymer chains (small α). In other words, the homopolymers becomes more efficient to swell the microphase separated structure for longer homopolymer chains (large α). Detailed free-energy analysis revealed that the stability of the lamellar phase is marginal for small block copolymer volume fraction. For $\alpha>1$, on the other hand, three-phase coexistence either between the disorder, A-rich and B-rich phases or between the lamellar, A-rich and B-rich phases is observed. © *2002 American Institute of Physics.* [DOI: 10.1063/1.1517038]

I. INTRODUCTION

A. Polymeric ternary systems

Traditional microemulsions being mixtures of oil, water, and surfactant, are known to exhibit various interesting microstructures depending on the temperature or the composition.[1,2] When the concentration of surfactant is relatively large, they show a rich variety of regularly ordered structures such as the cubic (gyroid) phase, the hexagonal phase, or the lamellar phase. By lowering the concentration of surfactant and if hydrophilic and lipophilic natures of the surfactant are balanced, microemulsions form a bicontinuous structure where a randomly oriented monolayer of surfactants separates oil-rich and water-rich subvolumes. A direct observation of the randomly intertwined structure by using the freeze-fracture microscopy has been reported.[3]

It has been widely recognized that mixtures of high molecular weight homopolymers and diblock copolymers are analogous to traditional microemulsions.[4,5] Similar to the low molecular weight surfactant molecules, AB diblock copolymers tend to locate at the interface between the two phases rich in A and B homopolymers. The emulsifying effect of copolymer added to blends of homopolymer was considered using Flory–Huggins theory and random phase approximation (RPA) by Leibler.[6,7] His theory was used to take into account the microphase separation of the ternary blends including block copolymers.[8,9] For the symmetric ternary case, the line of macrophase separation into A-rich and B-rich phases is connected to the line of microphase separation to the lamellar phase at the isotropic Lifshitz point (see Sec. II).[8,9]

On the basis of self-consistent field theory (SCFT), Noolandi and Hong showed that the copolymer chains lower the interfacial tension.[10,11] They showed that the reduction in interfacial tension increases with copolymer molecular weight and concentration. Their theory was extended by Shull and his co-workers to investigate the interfacial properties of ternary blends by performing the numerical treatment of the SCFT.[12–14] Banaszak and Whitmore calculated phase diagrams of ternary blends which undergo both microphase and macrophase separation on the basis of a fourth-order expansion.[15] Israels *et al.* examined the effect of diblock size relative to the homopolymers on the compatibilization of homopolymer blends.[16] They showed that interfacial tension can be reduced to zero if the blocks in the diblock are longer than the corresponding homopolymer. The Fourier-space SCFT calculations of ternary blends have been performed by Janert and Schick.[17,18] They investigated the influence of relative chain length on the phase behavior of the system.[17] The calculated phase diagrams include disordered, lamellar, hexagonal, and cubic phases, as well as two- and three-phase coexistence region. In their later paper, the unbinding nature of the system was discussed.[18] Upon dilu-

a)Electronic mail address: komura@comp.metro-u.ac.jp
b)Electronic mail address: kodama@rc.m-kagaku.co.jp

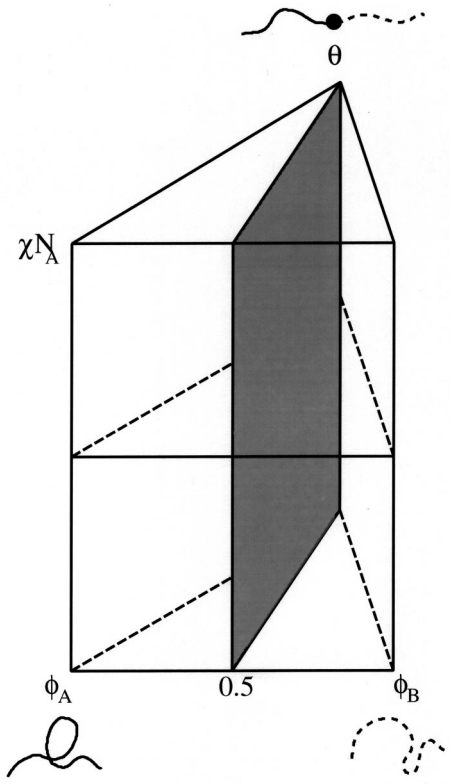

FIG. 1. The phase prism for a ternary blend of two homopolymers and a block copolymer. ϕ_A and ϕ_B are homopolymer volume fractions, and θ is the copolymer volume fraction. The vertical coordinate is the incompatibility degree χN_A. The shaded plane cut through the prism at $\phi_A=\phi_B$ is the isopleth.

tion by the homopolymers, the symmetric lamellar phase does not unbind, whereas it always becomes unstable to the asymmetric lamellar phases which do unbind.

B. Polymeric microemulsions

One of the most interesting experimental findings by Bates *et al.* in a polymeric ternary system is the existence of a bicontinuous structure without any long-range order (LRO).[19,20] The investigated system consists of nearly equal size poly(ethylene) (PE) and poly(ethylene propylene) (PEP) homopolymers and a symmetric PE–PEP diblock copolymer. They focused on the symmetric case in which the volume fractions of the two homopolymers are equal (see Fig. 1). By changing the average volume fraction of the copolymer θ, transmission electron microscopy (TEM) images revealed that a lamellar structure is observed for $\theta>\theta_L$ and a two-phase structure appears for $\theta<\theta_L$, where θ_L is the Lifshitz volume fraction. Images obtained from the specimens close to θ_L bear a striking resemblance to bicontinuous microemulsions in mixtures of oil, water, and surfactant. Such a new phase has been termed as ''polymeric microemulsions'' (PME). For different types of ternary systems, it is demonstrated that there is a common region in phase space over which bicontinuous PME is stable and the general phase behavior is rather universal.[21–24] In their works, the bicontinuous PME has been regarded as a disordered phase which is driven by fluctuations of lamellar phase.[19–21] To explain this, a singular cusp in the phase transition temperature is assumed as θ is varied about θ_L, and the region of the disordered phase is considered to extend to very low temperatures within this cusp.

Various theoretical approaches for PME have been addressed. Kielhorn and Muthukumar extended the mean-field theory by including composition fluctuations, and concluded that the Lifshitz point is destroyed due to the fluctuations.[25] Later, Kielhorn and Muthukumar derived a mean-field time-dependent Ginzburg–Landau equation to model the spinodal decomposition of polymeric ternary systems.[26] Matsen calculated the elastic properties of a diblock copolymer monolayer within SCFT,[27] and showed that the calculated bending modulus and saddle-splay modulus satisfy the conditions required to melt the lamellar phase. Using SCFT and strong-segregation theory, Thompson and Matsen have calculated the effective interactions between the copolymer monolayers.[28] From the condition that the attraction becomes sufficiently small, they concluded that the optimum size of the homopolymer molecules is about 80% that of the copolymer molecule. In a more recent paper, Thompson and Matsen predicted that copolymer polydispersity can improve PME by forming flexible and nonattractive monolayers.[29]

C. The present work

In this paper, using a lattice (real-space) SCFT method, we investigate the phase separated structure of the symmetric mixtures of A and B homopolymers plus AB diblock copolymers. Our purpose is to study the morphological change of the microphase separated structure when the total copolymer volume fraction or the relative chain lengths between the homopolymers and the diblock copolymer is varied systematically. We numerically solve the SCFT equations in a real space *without* assuming the symmetry of the structure *a priori* according to the method proposed by Hasegawa.[30] Application of this method for the polymeric ternary system and some of the preliminary results have been reported in our previous works.[31–33] This paper provides the detailed description of our results as well as more extended calculations. Independently, the real-space SCFT method has been used by other authors such as for linear $ABCA$ tetrablock copolymers,[34,35] or star and linear ABC triblock copolymers.[36] In general, this method proved to be a powerful tool in finding new mesophases either with or without LRO.[37]

Starting with randomly generated initial potential fields, we demonstrate that a bicontinuous structure similar to PME results from the microphase separation for relatively longer copolymer chain. For the fixed copolymer length, we find that the typical length scale of the microphase separated structure becomes smaller for relatively smaller homopolymer chains. For relatively longer homopolymer chains, we observed the three-phase coexistence either between the disorder, A-rich and B-rich phases or between the lamellar, A-rich and B-rich phases depending on the strength of the interaction parameter.

Since the obtained bicontinuous structure may correspond to metastable equilibrium, we have also performed the same calculation starting from the initial potential fields with

an imposed lamellar symmetry. By calculating the free energy of the lamellar phase as a function of the average volume fraction of the copolymer, we discuss the effective interactions between the copolymer monolayers. We find that there is a region where the stability of the lamellar phase is marginal.

This paper is constructed as follows. In the next section, the mean-field phase diagrams of the polymeric ternary system are explained within the RPA for various relative chain lengths. In Sec. III, we summarize the general formulation of the real-space SCFT for a system including copolymers, and describe the numerical procedure based on the lattice version of SCFT. Section IV gives the analysis of our simulation results. Summary and conclusion are provided in Sec. V. Details of the general formulation and some technical remarks are given in Appendix A. Appendix B describes the iteration scheme to solve the set of self-consistent equations.

II. RANDOM PHASE APPROXIMATION

A. Notations

In general, we consider a ternary blend of A and B homopolymer of polymerization indices N_A and N_B, respectively, and AB diblock copolymer of polymerization index N_{AB} of which a fraction f consists of A monomer. Then, we introduce two dimensionless parameters defined by

$$\alpha_A \equiv \frac{N_A}{N_{AB}}, \quad \alpha_B \equiv \frac{N_B}{N_{AB}}, \tag{2.1}$$

respectively. The volume fractions of A and B homopolymers are denoted by $\phi_A(\mathbf{r})$ and $\phi_B(\mathbf{r})$, respectively, and the volume fraction of AB block copolymer by $\phi_{AB}(\mathbf{r})$. In addition, $\phi_a(\mathbf{r})$ and $\phi_b(\mathbf{r})$ represent the volume fractions of A and B blocks in the AB block copolymer, respectively. The average volume fraction of each component is indicated with a bar, such as $\overline{\phi}_A$, $\overline{\phi}_B$, or $\overline{\phi}_{AB} \equiv \theta$. We assume that the system is incompressible, i.e.,

$$\phi_A + \phi_B + \phi_a + \phi_b = 1. \tag{2.2}$$

Due to this constraint, we define the following three quantities as independent order parameters:

$$\Phi \equiv \phi_A - \phi_B, \tag{2.3}$$

$$\Psi \equiv \phi_a - \phi_b, \tag{2.4}$$

$$\Delta \equiv \phi_A + \phi_a - \phi_B - \phi_b. \tag{2.5}$$

The last order parameter represents the difference in the volume fractions of all A and B monomers. The Flory–Huggins interaction parameter between A and B segments is denoted by $\chi_{AB} \equiv \chi$.

The phase behavior of a polymeric ternary blend can be represented in the form of a phase prism shown in Fig. 1. Within the large parameter space, we focus on the symmetric case, namely (i) both A and B homopolymers have the same length ($N_A = N_B$ and hence $\alpha_A = \alpha_B \equiv \alpha$); (ii) the AB block copolymer contains A and B monomers in equal proportions ($f = 1/2$); and (iii) the average volume fractions of A and B homopolymers are equal and determined by

$$\overline{\phi}_A = \overline{\phi}_B = \frac{1-\theta}{2}. \tag{2.6}$$

In other words, we consider the isopleth (shaded plane in Fig. 1) in the phase prism.

B. Correlation function

Here, we discuss the phase behavior of polymeric ternary systems within the random phase approximation (RPA) for various values of α. Mean-field phase diagram on the isopleth for $\alpha = 1$ was considered by Leibler,[6,7] and later calculated for $\alpha \neq 1$ by Broseta and Fredrickson.[8] The essential part of the phase diagram can be obtained by looking at the monomer concentration correlation function (structure factor). Within the RPA, Leibler calculated the correlation function for Φ as[7]

$$S_{\Phi\Phi}(x) = \frac{2S_A(x)\{1-\chi[S_{AA}(x)-S_{AB}(x)]\}}{1-\chi[S_A(x)+S_{AA}(x)-S_{AB}(x)]}. \tag{2.7}$$

Here, $x = (qR)^2 = q^2 N_A b^2/6$, where $q = |\mathbf{q}|$ is the absolute value of the wave vector $\mathbf{q}$, R is the radius of gyration, and b is the statistical segment length. In the above, $S_A(x)$ is the correlation function of independent A homopolymer, $S_{AA}(x)$ and $S_{AB}(x)$ are $A-A$ and $A-B$ monomers correlation functions of independent copolymer chains. These are given by

$$S_A(x) = \frac{1-\theta}{2} N_A g(1,x), \tag{2.8}$$

$$S_{AA}(x) = \frac{\theta N_A}{\alpha} g\left(\frac{1}{2}, \frac{x}{\alpha}\right), \tag{2.9}$$

$$S_{AB}(x) = \frac{\theta N_A}{\alpha}\left[\frac{1}{2} g\left(1, \frac{x}{\alpha}\right) - g\left(\frac{1}{2}, \frac{x}{\alpha}\right)\right], \tag{2.10}$$

where $g(h,x)$ is the Debye function defined by

$$g(h,x) = \frac{2}{x^2}(hx + e^{-hx} - 1). \tag{2.11}$$

The limit of stability of the disordered phase occurs for the smallest value of $\chi(x)$ (highest temperature) at which (2.7) diverges. From (2.7) to (2.11), this condition is written as

$$\frac{1}{\chi(x) N_A} = \frac{1}{x^2}[-1 + x + e^{-x} + \theta\{1 - e^{-x} + \alpha(-3 + 4e^{-x/2\alpha} - e^{-x/\alpha})\}]. \tag{2.12}$$

When $\alpha = 1$, this equation reduces to Eq. (3.2) in Ref. 9. Minimizing $\chi(x)$ with respect to x, we see that for $0 < \theta < 2\alpha^2/(1+2\alpha^2)$, the minimum occurs at $x = 0$ and the corresponding value is

$$\frac{1}{\chi N_A} = \frac{1-\theta}{2}. \tag{2.13}$$

This is called the "Scott line" (consolute line) along which the disordered phase makes a continuous transition to coexisting uniform ($q = 0$) phases. The system exhibits the mac-

rophase separation between A-rich and B-rich phases. For $2\alpha^2/(1+2\alpha^2)<\theta<1$, the instability occurs at a nonzero value of x. This case corresponds to the microphase separation to a lamellar phase. When the transition to the lamellar phase ($q\neq 0$) occurs, the density of the copolymer is given by

$$\theta(x)=[-2+x+(x+2)e^{-x}]/[6\alpha-2+(x+2)e^{-x}+(x+2\alpha)e^{-x/\alpha}-2(x+4\alpha)e^{-x/2\alpha}], \tag{2.14}$$

and the transition line is located according to (2.12) with (2.14). It is important to note that (2.14) holds only for $0<x\leqslant 3.785$.[9] The point which connects the macrophase and microphase transition lines is known as an isotropic ($m=d$, where m is the number of dimensions in which wave vector instability occurs, and d is the space dimension) Lifshitz point[8,38]

$$\theta_{\mathrm{L}}=\frac{2\alpha^2}{1+2\alpha^2},\quad (\chi N_A)_{\mathrm{L}}=2(1+2\alpha^2). \tag{2.15}$$

It is instructive to derive the Ginzburg–Landau (GL) free energy from the obtained correlation function. By expanding $S_{\Phi\Phi}^{-1}$ in (2.7) for small q, we obtain the free energy $F[\Phi]$ as

$$F_{\mathrm{GL}}[\Phi]\approx\frac{\rho_0}{2N_A}\int d\mathbf{r}[c(\nabla^2\Phi)^2+g(\nabla\Phi)^2+t\Phi^2], \tag{2.16}$$

where ρ_0 is the monomer density and the coefficients are

$$c=\frac{1}{36}\left[\frac{1}{1-\theta}+\frac{9(\chi N_A)^2\theta}{16\alpha^3}-\frac{(\chi N_A)^3\theta^2}{8\alpha^4}\right]R^4, \tag{2.17}$$

$$g=\frac{1}{3}\left[\frac{1}{1-\theta}-\frac{(\chi N_A)^2\theta}{8\alpha^2}\right]R^2, \tag{2.18}$$

$$t=\frac{1}{1-\theta}-\frac{\chi N_A}{2}. \tag{2.19}$$

Throughout this paper, all the energies are expressed in units of k_BT, where k_B and T represent the Boltzmann constant and the temperature, respectively. Notice that the Scott line (2.13) is determined from the condition $t=0$. On the other hand, the phase boundary between the lamellar and the two-phase coexisting region is determined from the relation[39]

$$2(2-\sqrt{6})a=g^2/c, \tag{2.20}$$

within the GL expansion. It important to note that this relation holds only close to the critical point where the expansion is justified. We comment here that when $c,t>0$ and $g<0$, (2.16) is the free energy of traditional microemulsions proposed by Teubner and Strey.[40] In this case, $\Phi(\mathbf{r})$ is defined as an order parameter which measures the local difference in volume fractions between oil and water.

In addition to these phase boundaries, one can locate the ''disorder line'' and the ''Lifshitz line'' in the disordered region of the phase diagram.[9] The disorder line is the locus of points at which the asymptotic behavior of the correlation function changes from a monotonic exponential decay to an exponentially damped oscillatory decay. This oscillatory behavior reflects the tendency of the copolymer to order the homopolymers. The disorder line can be calculated from (2.12) and (2.14) by setting $x=-y$, where y ranges over all positive real numbers ($y>0$). On the other hand, the Lifshitz line is the locus of points at which the oscillations are sufficient to produce the dominant peak in the associated structure function at nonzero wave vector. The Lifshitz line for the Φ–Φ structure function $S_{\Phi\Phi}$ [see (2.7)] is obtained by setting $g=0$ in (2.18), and one obtains

$$\frac{1}{\chi N_A}=\left[\frac{(1-\theta)\theta}{8\alpha^2}\right]^{1/2}. \tag{2.21}$$

However, another situation occurs as θ is increased. The Lifshitz line is connected to the ''equimaxima line'' at which the two peaks (one at $q=0$, and the other at $q\neq 0$) in the structure function become of equal height.[9]

Phase diagrams on the isopleth for $\alpha=0.25$, 0.5, and 1 including several different lines are shown in Fig. 2. Notice that Fig. 2(c) is the same as Fig. 3 in Ref. 9. The Scott lines start from $(\theta,\chi N_A)=(0,2)$ (point C), whereas the lines of microphase separation end at $(\theta,\chi N_A)=(1,10.5\alpha)$ (point G). Disorder lines start from (0,0) (point D) except for $\alpha=1$. The transition line between the lamellar and the two-phase coexistence region is drawn only near the Lifshitz point where the GL expansion is valid. According to Fig. 2(c) ($\alpha=1$), Holyst and Schick concluded that the copolymer is inefficient in the organization of homopolymers since the Lifshitz line (line LE) is far from the disorder line (line LD). However, this tendency changes as α is decreased from 1. We see that the Lifshitz line appears even in the small copolymer volume fraction region such as in Fig. 2(a). In the experiment by Bates *et al.*, the parameter α was chosen as $\alpha\sim 0.2$ in order to ensure that both the points C and G in the phase diagram can be explored over the similar temperature window.[19,21,22]

C. Multiphase coexistence

It is important to notice that the above discussion is valid only for $\alpha\leqslant 1$. For $\alpha>1$, the Lifshitz point is preempted by a tricritical point[8]

$$\theta_{\mathrm{TCP}}=\frac{2\alpha}{1+2\alpha},\quad (\chi N_A)_{\mathrm{TCP}}=2(1+2\alpha). \tag{2.22}$$

Notice that $(\chi N_A)_{\mathrm{TCP}}<(\chi N_A)_{\mathrm{L}}$ for $\alpha>1$. The special case of $\alpha=1$ corresponds to a ''Lifshitz tricritical point,'' as has been pointed out in Refs. 8 and 9. The tricritical point indicates a continuous segregation into three phases; two homopolymer-rich phases and a copolymer-rich lamellar phase.

A typical phase diagram for $\alpha=2$ is calculated in Fig. 3. For small θ, the disordered phase undergoes a continuous transition to A- and B-rich uniform phases at the Scott line (2.13). This line ends at a tricritical point (2.22), beyond which is a line (triple line) of three-phase coexistence between A-rich, B-rich, and disordered block copolymer phases. The region of three-phase coexistence can be calculated within the Flory–Huggins approximation where the reduced free energy is given by[8]

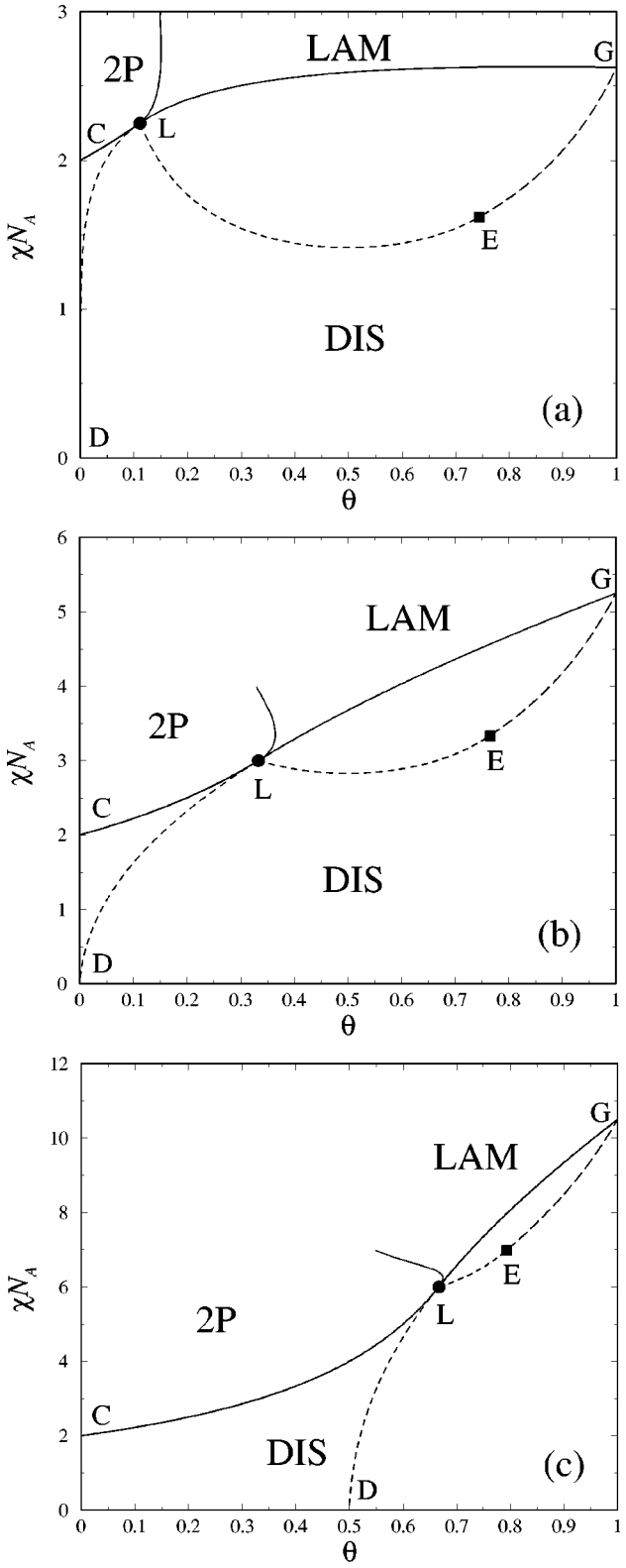

FIG. 2. Phase diagrams of the symmetric ternary mixture for (a) $\alpha = N_A/N_{AB} = 0.25$; (b) $\alpha = 0.5$; and (c) $\alpha = 1$ as obtained from the random phase approximation. θ is the total volume fraction of the copolymer. The regions labeled LAM, DIS, and 2P are, respectively, regions of lamellar, disordered, and two-phase coexisting phases. L is the Lifshitz point. The line CL is that of continuous transition from the disordered phase to coexisting *A*-rich and *B*-rich phases, LG is the line of continuous transitions from the disordered phase to the lamellar phase, LD is the disorder line, and LE and EG are the Lifshitz and equimaxima lines for the Φ–Φ structure function, respectively.

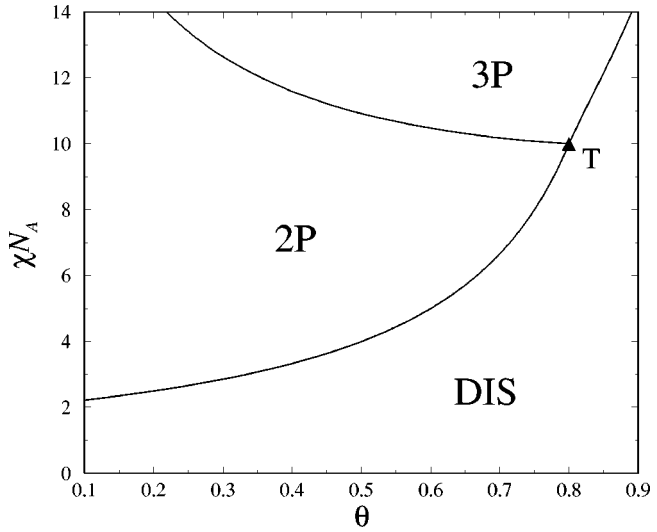

FIG. 3. Phase diagram of the symmetric ternary mixture for $\alpha = N_A/N_{AB} = 2$. In addition to the notations given in Fig. 2, the region labeled 3P is the region of three-phase coexistence between *A*-rich, *B*-rich, and disordered block copolymer phases. T is the tricritical point.

$$f(\Phi,\theta) = \frac{1-\theta+\Phi}{2}\log(1-\theta+\Phi) + \frac{1-\theta-\Phi}{2}\log(1-\theta-\Phi) + \alpha\theta\log\theta - \frac{\chi N_A \Phi^2}{4}. \tag{2.23}$$

The compositions Φ and θ of the three coexisting phases are obtained by equating the chemical potentials of each species

$$\mu_\Phi = \frac{\partial f}{\partial \Phi}, \tag{2.24}$$

$$\mu_\theta = \frac{\partial f}{\partial \theta}, \tag{2.25}$$

and the osmotic pressure

$$\Pi = f - \mu_\Phi - \mu_\theta. \tag{2.26}$$

The triple line terminates at a four-phase point at which the lamellar phase coexists with the other three phases.[41] Beyond this point, there is a direct transition line between the disordered phase and the lamellar phase. These regions are not shown in Fig. 3.

III. LATTICE SELF-CONSISTENT FIELD THEORY

A. Self-consistent field theory

Self-consistent field theory (SCFT) in polymer science originates from the early works by Edwards[42] or by Helfand and Tagami.[43] The basic idea of SCFT is as follows: polymers are represented as random walks in a positional dependent segment potential, which depends in a self-consistent way on the distribution of segments. SCFT has been applied to various problems and its recent achievements are summarized such as in Refs. 37 and 44. In fact, the RPA used in the previous section is one of the approximated formulations of SCFT.

There are, basically, two possible ways to formulate the SCFT: Fourier-space and real space representations. Recently, the Fourier-space SCFT method proved to be quite useful to predict the phase diagram of block copolymer melts.[45,46] In this method the set of self-consistent equations is solved by using a restricted Fourier basis appropriate for an assumed mesophase symmetry. Later, various periodic structures with LRO were successfully explained within the SCFT for polymeric ternary systems.[15,17,18] In these works, the free energies of several periodic structures were calculated by assuming their mesophase symmetry *a priori*.

On the other hand, the set of self-consistent equations (see the next subsection) can be solved also in a real space. This real-space method was initiated by Scheutjens and Fleer as a lattice version of SCFT,[47] and has been further developed for surface problems with specific boundary conditions.[48,49] More recent works using the real-space (both lattice and off-lattice) SCFT are given in Ref. 50.

Furthermore, it is advantageous in the real-space method that one need not assume the symmetry of structures *a priori*.[31–37] In order not to bias the symmetry of patterns that emerges, one numerically solves the self-consistent equations by starting with random potential fields. Although this method may generate the structures corresponding to either stable or metastable equilibrium, it has proved to be a powerful tool in finding new mesophases. A similar approach was taken in Ref. 16, in which they observed droplet microemulsions. In the present paper, we employ the real-space lattice SCFT with a slight extension of the previous method.

B. Self-consistent equations in the lattice formulation

Here, we give the set of self-consistent equations in the lattice formulation of SCFT which is essentially based on Refs. 48 and 49. While Ref. 48 treats only surface adsorption problems, we apply the lattice SCFT to higher space dimensions. Although there are many derivations of SCFT, we give the details of the lattice formulation in Appendix A for the completeness of our paper. Notice that the present lattice formulation is not a simple discretization of the continuum model.

The space coordinate of each segment composing the polymers is specified by a lattice point $\mathbf{n}=(n_x,n_y,n_z)$ in an $L_x\times L_y\times L_z(\equiv\Omega)$ cubic lattice box with a lattice constant a. We denote the type of molecule by i, and the type of segment by J and K. (In the present case, $i=A,B$ for A and B homopolymers, and $i=AB$ for AB copolymer, whereas J or K points to either A or B segment.) Segments in a chain are indexed by $N'=1,2,\ldots,N_i$, where N_i is the polymerization index of the ith molecule. The molecules of type i are indexed by $p=1,2,\ldots,n_i$, where n_i is the total number of ith molecule.

We introduce two Green's functions $G_i(\mathbf{n},N')$ and $G_i^\dagger(\mathbf{n},N')$ for walks starting at $N'=1$ and N_i, respectively. These functions obey the following recursive relations:

$$G_i(\mathbf{n},N')=\exp[-U_{f_i(N')}(\mathbf{n})]\langle\langle G_i(\mathbf{n}',N'-1)\rangle\rangle, \tag{3.1}$$

$$G_i^\dagger(\mathbf{n},N')=\exp[-U_{f_i(N')}(\mathbf{n})]\langle\langle G_i^\dagger(\mathbf{n}',N'+1)\rangle\rangle, \tag{3.2}$$

together with the initial conditions

$$G_i(\mathbf{n},1)=\exp[-U_{f_i(1)}(\mathbf{n})], \tag{3.3}$$

$$G_i^\dagger(\mathbf{n},N_i)=\exp[-U_{f_i(N_i)}(\mathbf{n})]. \tag{3.4}$$

Here, $f_i(N')$ is the "type function" representing the type of the segment N' in the ith chain, and $\langle\langle\cdots\rangle\rangle$ denotes a neighborhood average defined later by (3.9). The segment potential is given by

$$U_J(\mathbf{n})=u(\mathbf{n})+\sum_K \chi_{JK}\langle\langle\phi_K(\mathbf{n})\rangle\rangle, \tag{3.5}$$

where χ_{JK} is the Flory–Huggins parameter between J and K segments. Physically, $u(\mathbf{n})$ represents an entropic hard-core potential which is independent of the segment type, whereas the second term is the interaction part. The segment distribution function in (3.5) is expressed as

$$\phi_J(\mathbf{n})=\sum_i\sum_{N'=1}^{N_i}\delta[J,f_i(N')]\phi_{i,N'}(\mathbf{n}), \tag{3.6}$$

with

$$\phi_{i,N'}(\mathbf{n})=\frac{n_iG_i(\mathbf{n},N')G_i^\dagger(\mathbf{n},N')}{\exp[-U_{f_i(N')}(\mathbf{n})]\Sigma_{\mathbf{n}'}G_i(\mathbf{n}',N_i)}, \tag{3.7}$$

where $\delta[J,f_i(N')]$ is a Kronecker delta with value 1 if segment $f_i(N')$ is of type J, and 0 otherwise. Equation (3.7) is called the "composition law." Finally, the incompressibility condition requires that

$$\sum_J \phi_J(\mathbf{n})=1, \tag{3.8}$$

holds at any site. From (3.1) to (3.8) forms a set of self-consistent equations to be solved for $\{\phi_J(\mathbf{n})\}$ and $\{U_J(\mathbf{n})\}$.

Up to now, the formulation is rather general and standard. In order to avoid the geometric constraints associated with a lattice, the neighborhood average $\langle\langle\cdots\rangle\rangle$ in (3.1), (3.2), or (3.5) is taken according to[51]

$$\langle\langle X(\mathbf{n})\rangle\rangle=\sum_{\mathbf{n}'}\left[\frac{6}{80}\delta[|\mathbf{n}-\mathbf{n}'|^2,1]+\frac{3}{80}\delta[|\mathbf{n}-\mathbf{n}'|^2,2]+\frac{1}{80}\delta[|\mathbf{n}-\mathbf{n}'|^2,3]\right]X(\mathbf{n}'). \tag{3.9}$$

This type of neighborhood average has the desirable property of being more generally isotropic, and is a natural extension of the standard nearest-neighbor average given by (A5). See also the corresponding ideal Hamiltonian (A29). On the other hand, (3.9) has been successfully used in the cell-dynamical simulations.[51] A related discussion is provided in Ref. 52 in which the coefficients in (3.9) are carefully determined in order to be consistent with the Gaussian chain model in a continuum treatment.

After solving these equations, we calculate the mixing free energy F_m with respect to the unmixed pure reference system where the segment interactions are switched off. Then, we have

TABLE I. Characterization of the symmetric polymeric ternary systems for the fixed copolymer length case ($\alpha \leqslant 1$).

System	$N_A=N_B$	N_{AB}	α	χ	$\chi N_A=\chi N_B$	χN_{AB}	$(\theta_L,(\chi N_A)_L)$
system 1 (S1)	2	8	0.25	2	4	16	(1/9, 9/4)
system 2 (S2)	4	8	0.5	2	8	16	(1/3, 3)
system 3 (S3=S6)	8	8	1	2	16	16	(2/3, 6)

$$F_m[\phi_J,U_J]=\sum_i n_i \log \frac{n_i N_i}{\Sigma_{\mathbf{n}} G_i(\mathbf{n},N_i)} + \frac{1}{2}\sum_{\mathbf{n}} \sum_{J,K} \chi_{JK}\phi_J(\mathbf{n})\langle\langle \phi_K(\mathbf{n})\rangle\rangle - \sum_{\mathbf{n}} \sum_J U_J(\mathbf{n})\phi_J(\mathbf{n}). \quad (3.10)$$

C. Numerical procedure

The above set of self-consistent equations is solved in the following way.[30,48,49] We first give an initial guess for $\{U_J(\mathbf{n})\}$ which can be either random or periodic in space. In general, we do not need to assume any symmetry of the structure *a priori*, which differs from the Fourier-space treatment of SCFT such as in Refs. 45 and 46. Then, we compute the single chain statistical weights $G_i(\mathbf{n},N')$ and $G_i^{\dagger}(\mathbf{n},N')$ from (3.1) and (3.2), respectively. Using these quantities, we obtain the distribution $\{\phi_{i,N'}(\mathbf{n})\}$ from (3.7). Then, $\phi_J(\mathbf{n})$ is calculated by (3.6). At this point, we examine whether the incompressibility condition (3.8) is satisfied, and whether the segment potential gives the same $u(\mathbf{n})$ for each segment type. If these constraints are satisfied, the initial estimate corresponds to equilibrium. Otherwise, new estimates for $\{U_J(\mathbf{n})\}$ are made until the conditions are met. Notice that the present algorithm is not intended to mimic real polymer dynamics, but is an efficient artifice to evolve a system as fast as possible to a free-energy minimum which can be either stable or metastable. The details of the Picard-type iteration scheme used is presented in Appendix B.

First, we numerically solve the set of SCFT equations starting with randomly generated potential fields. This simulation is performed in 2D ($L_x=L_y=256$, $L_z=1$) and 3D ($L_x=L_y=L_z=64$) systems. In 2D cases, we neglect any gradients in the z-direction and put[53]

$$X(n_x,n_y,n_z-1)=X(n_x,n_y,n_z+1)=X(n_x,n_y,n_z). \quad (3.11)$$

Furthermore, the periodic boundary condition is imposed. As in Sec. II, we only consider the interaction between the A and B segments

$$\chi_{AB}=\chi_{BA}=\chi. \quad (3.12)$$

Notice that although the present method may not be suitable for determining the fully equilibrated structures, it enables us to generate a structure which does not possess any LRO such as PME as a metastable structure. Since the obtained patterns may depend on the initially prepared potential fields, we also study 1D systems starting with 1D periodic potential fields. The latter case yields lamellar structures with a well-defined periodicity. We chose different parameters for 1D and 2D calculations in order to maximize the computational efficiency for large 2D systems.

IV. RESULTS AND DISCUSSION

In this section, we present our results of simulations described previously. We focus here on the symmetric case as in Sec. II, and examine the influence of the relative chain length between homopolymers and copolymer. We did it in two ways; one by fixing the copolymer length and changing the homopolymer length, and the other by fixing the homopolymer length and changing the copolymer length. Some preliminary results for $\alpha>1$ case and 3D system are also reported. All the results from Sec. IV A to IV D are obtained starting with randomly generated potential fields without assuming any symmetry, whereas Sec. IV E treats the case starting from 1D periodic initial conditions.

A. Fixed copolymer length ($\alpha \leqslant 1$)

We first discuss the case where the length of AB block copolymer is fixed to $A4B4$ ($N_{AB}=8$), whereas lengths of both A and B homopolymers are changed. Three different homopolymer lengths are considered, which we refer to as systems 1, 2, 3 (or S1, S2, S3) as listed in Table I. For each homopolymer length, the average volume fraction of the copolymer θ ($=\overline{\phi}_{AB}$) is varied between 0 and 1. The interaction parameter between A and B monomers is fixed to $\chi=2$. Hence, the degree of incompatibility is fixed to $\chi N_{AB}=16$, which corresponds to the temperature below the microphase separation temperature $(\chi N_{AB})_{MST}\approx 10.5$ for $\theta=1$.[54] The typical patterns obtained from 2D simulations are depicted in Figs. 4 and 5 for S1 and S3, respectively. The volume fractions ϕ_A, ϕ_B, ϕ_a, and ϕ_b as defined in Sec. II are drawn in gray scale for five different copolymer volume fractions $\theta=0.1$, 0.3, 0.5, 0.7, and 0.9. Here, the values 0 and 1 correspond to white and black, respectively. In Fig. 6, we plotted the part of cross-section profiles of Φ and Ψ [see (2.3) and (2.4)] for $\theta=0.1$, 0.5, and 0.9 obtained from S3.

For small θ, there are large regions of A and B homopolymer rich domains. As can be clearly seen from Fig. 6(a), the profile of Φ changes sharply from -1 to 1 at the interface between the A-rich and B-rich domains. Most of the copolymers are located at the interface, and form saturated monolayers without any LRO. As θ is increased, the domain size becomes smaller and the amount of the interface increases, although the LRO still does not exist. Moreover, the difference between the maximum and the minimum values of Φ becomes smaller. This is due to the fact that the homopolymers are excluded by the copolymer brushes which

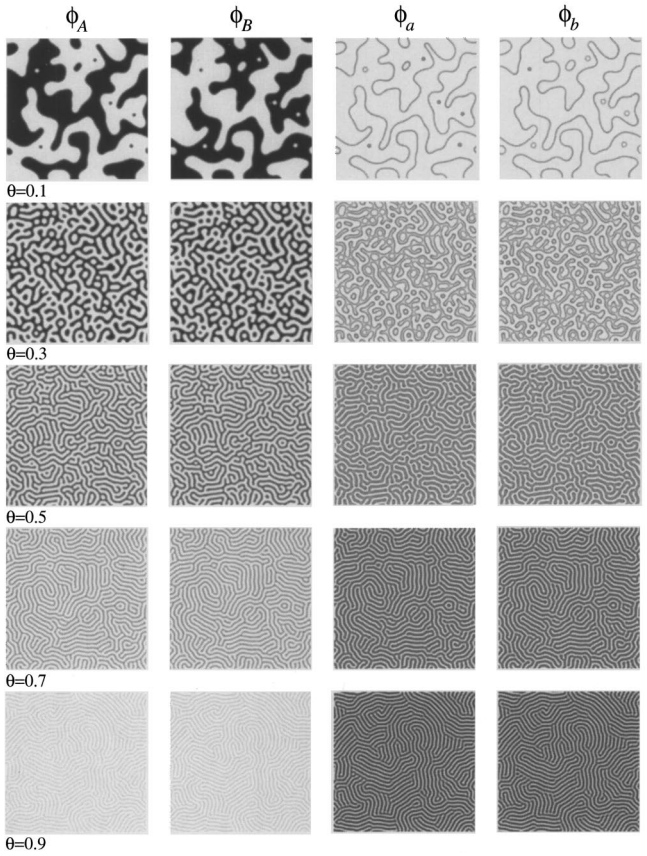

FIG. 4. Final patterns of system 1 in Table I for different values of θ drawn in gray scale. The values 0 and 1 correspond to white and black, respectively. ϕ_A and ϕ_B are volume fractions of A and B homopolymers, and ϕ_a and ϕ_b are the volume fractions of A and B blocks in the copolymer, respectively.

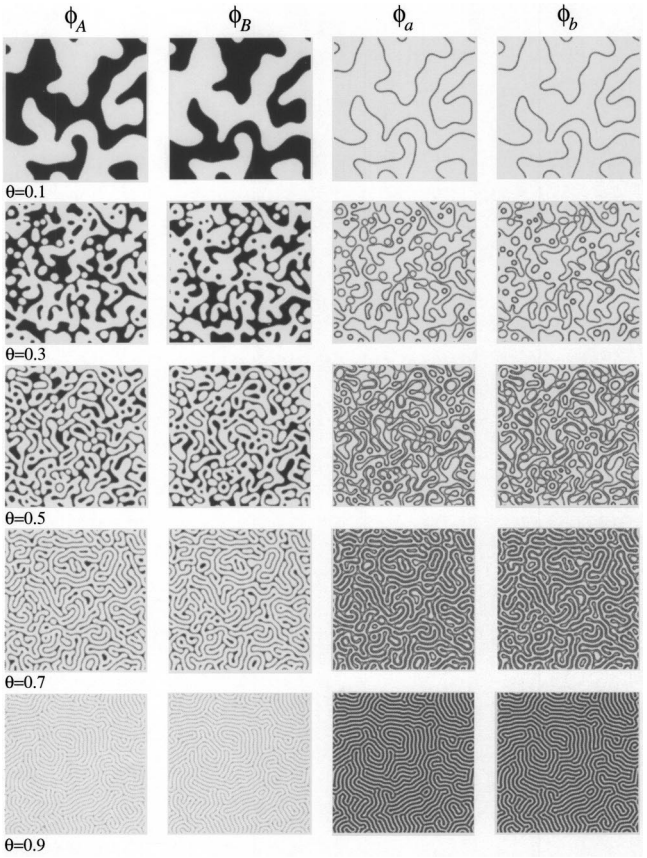

FIG. 5. Final patterns of system 3 in Table I. Notations are the same as those given in Fig. 4.

start to overlap. When θ is relatively large, the system exhibits a lamellar structure (with many defects) which is swollen by the small fraction of homopolymer chains. The lamellar structure can also be clearly seen in Fig. 6(c).

Both in Figs. 4 and 5, bicontinuous structures without any LRO appear below the transition temperature. Notice that in the present simulation, the effect of fluctuation is not included except for the initial random distribution of segment potential. We remark that there is a resemblance between the sequence of patterns shown here and those of PME obtained from the TEM micrographs[19] as θ is varied. In order to discuss the stability of PME, one needs to know, for example, the entropic contribution due to the random configuration of interfaces, which is balanced with their bending energy.[27] Of course, this is beyond the scope of the present mean-field approach. However, our result with random initial conditions shows, at least in the static sense, that PME with random configuration of interfaces results from microphase separation as metastable equilibrium. Notice that even the experimentally obtained PME may not necessarily be fully equilibrated structure. Interestingly, many holes observed in the A-rich and B-rich domains in the experiment [Fig. 3(d) in Ref. 19] are also reproduced such as in $\theta=0.1$ in Fig. 4 or $\theta=0.3$ in Fig. 5. These holes should be due to the emulsification of homopolymers by block copolymers.

In order to analyze the obtained patterns quantitatively, we pay attention to the behavior of Δ given in (2.5). First, we define a discrete Fourier transform of $\Delta(\mathbf{n})$ by

$$\Delta[\mathbf{k}]=\sum_{\mathbf{n}} \Delta(\mathbf{n})\exp(i\mathbf{k}\cdot\mathbf{n}), \tag{4.1}$$

with $\mathbf{k}=2\pi\mathbf{m}/L$, $\mathbf{m}\in\{0,1,\ldots,L-1\}^2$, and L is the system size. Then, the structure factor is given by

$$S(\mathbf{k})=\langle\Delta[\mathbf{k}]\Delta[-\mathbf{k}]\rangle, \tag{4.2}$$

where the average is over the ensemble of systems. Figure 7 shows the circularly averaged structure factor $S(k)$ ($k=|\mathbf{k}|$) of S3 for several values of θ ranging from $\theta=0.2$ to 1. Structure factors for $\theta=0$ and 0.1 are not shown here because their peak heights are much larger than those plotted in the graph. The peak height decreases as θ is increased at least up to $\theta=0.5$. This reflects the fact that the contrast between overall A and B segments becomes smaller. Above this value, the peak height gradually increases up to $\theta=1$.

By increasing θ from 0 to 1, the peak position shifts systematically to higher values of the wave vector. The peak position characterizes the typical length scale of each pattern. To see this in more detail, we calculate the (inverse) characteristic length scale defined by[51]

$$\langle k\rangle=\frac{\Sigma_{\mathbf{k}\neq\mathbf{0}}|\mathbf{k}|^{-1}S(\mathbf{k})}{\Sigma_{\mathbf{k}\neq\mathbf{0}}|\mathbf{k}|^{-2}S(\mathbf{k})}. \tag{4.3}$$

In Fig. 8, $\langle k\rangle$ is plotted as a function of θ for S1, S2, and S3 simultaneously. Although the homopolymer lengths are dif-

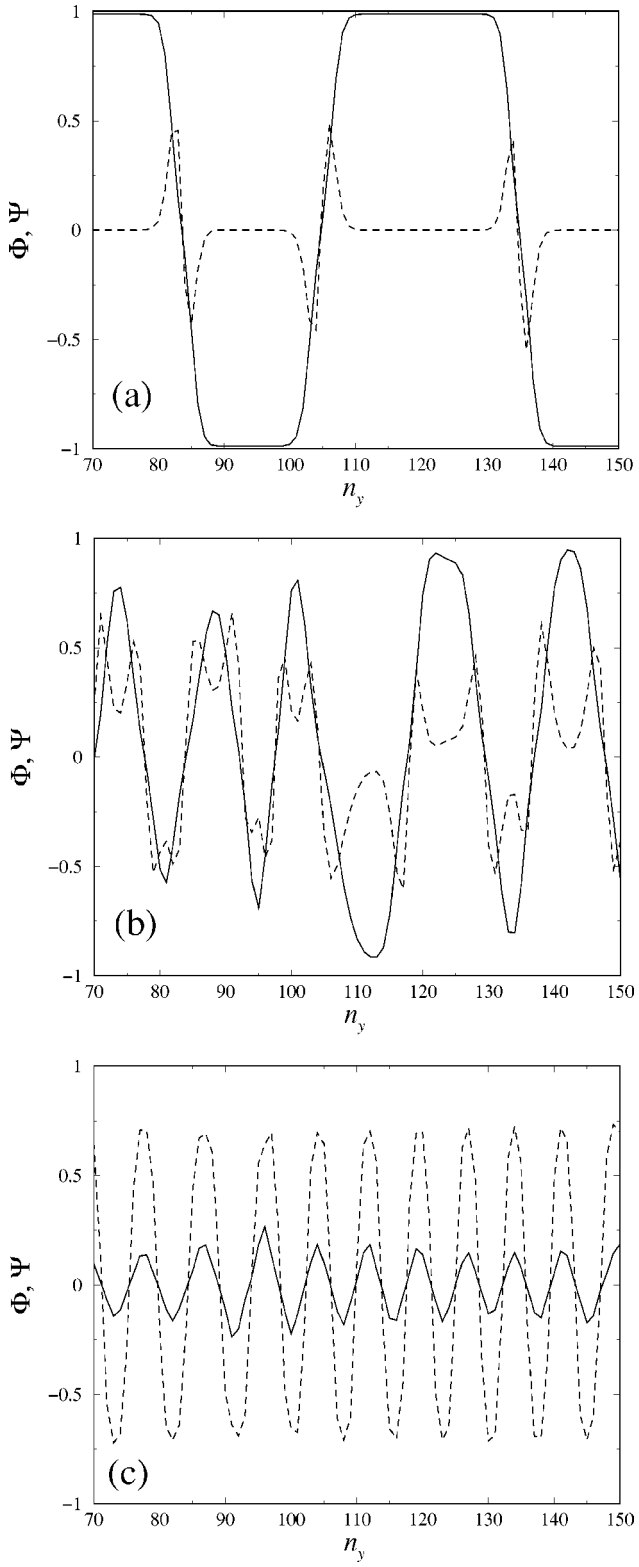

FIG. 6. Part of the cross-section profiles of Φ and Ψ for (a) $\theta=0.1$; (b) $\theta=0.5$; (c) $\theta=0.9$ of system 3 in Table I.

ferent for these three systems, the values of $\langle k\rangle$ at $\theta=0$ are the same. (In principle, macrophase separation takes place for $\langle k\rangle=0$. Finite value of $\langle k\rangle$ for $\theta=0$ in our simulation is due to the finite system size effect.) For $0<\theta<1$, $\langle k\rangle$ is larger for relatively longer copolymer chain (smaller α). This result indicates that the homopolymers becomes more efficient to swell the microphase separated structure by choosing larger α. In other words, the homopolymer chains penetrate into the copolymer brushes for small α.[14] However, it should be noted that this tendency is true as long as the system is not too close to the unbinding transition point at which the lamellar spacing diverges upon dilution by homopolymers.

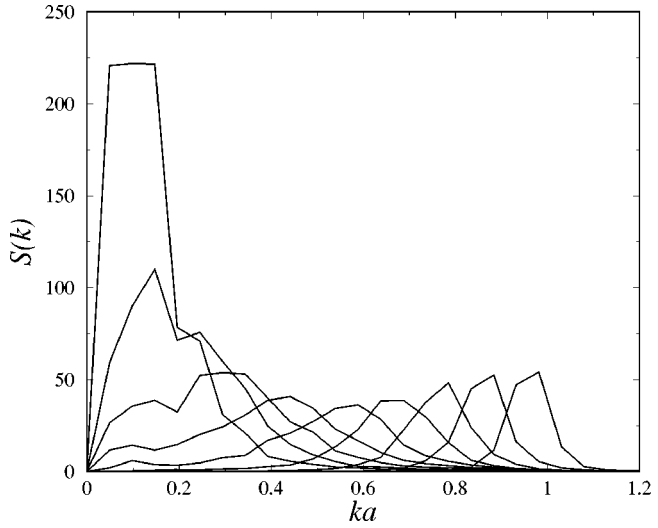

FIG. 7. Circularly averaged structure factor for different values of θ of system 3 in Table I. $\theta=0.2, 0.3,\ldots,1.0$ from left to right peaks.

Since we do not know of a systematic experimental study on the polymeric ternary system, we compare our results with the experiment on the traditional microemulsions. The structure of one-phase AOT/D_2O/decane microemulsions containing equal volumes of water and oil and a variable concentration of surfactant was investigated by Kotlarchyk *et al.* using SANS.[55] They found that as the volume fraction of AOT is increased from 0.18 to 0.42, the peak position exhibits an approximately linear shift to larger values of wave vector, while the peak height rapidly diminishes.

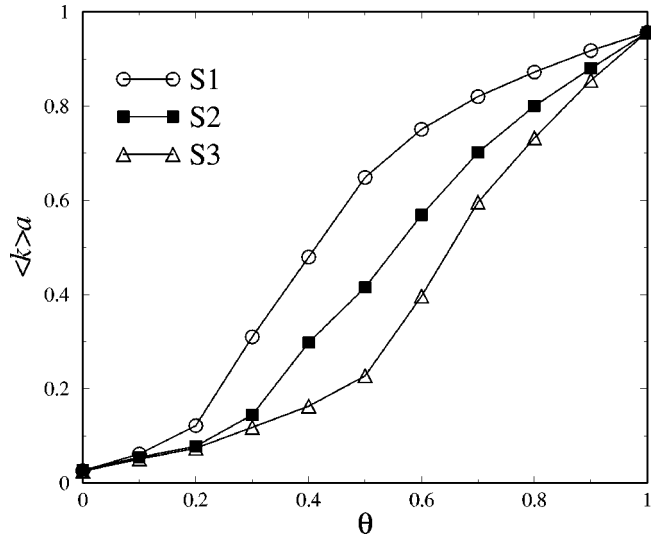

FIG. 8. The inverse characteristic length as a function of θ for systems 1, 2, and 3 in Table I which have the same copolymer length but different homopolymer length.

TABLE II. Characterization of the symmetric polymeric ternary systems for the fixed homopolymer length case ($\alpha \leqslant 1$).

System	$N_A=N_B$	N_{AB}	α	χ	$\chi N_A=\chi N_B$	χN_{AB}	$(\theta_L,(\chi N_A)_L)$
system 4 (S4)	8	32	0.25	2	16	64	(1/9, 9/4)
system 5 (S5)	8	16	0.5	2	16	32	(1/3, 3)
system 6 (S6=S3)	8	8	1	2	16	16	(2/3, 6)

The latter observation is in accord with our results in Fig. 7 for $\theta<0.5$. However, the behavior of $\langle k\rangle$ depends on α in the polymeric systems (see Fig. 8).

B. Fixed homopolymer length ($\alpha \leqslant 1$)

Next, we fix both of the homopolymer lengths to $N_A=N_B=8$, and change the copolymer length N_{AB}. Three different copolymer lengths are considered as in Table II, which we refer to as systems 4, 5, 6 (or S4, S5, S6). Notice that S6 is identical to S3. The interaction parameter is fixed to $\chi=2$, i.e., the degree of incompatibility is set to $\chi N_A=16$.

The sequences of patterns of S4, S5, and S6 ($\alpha \leqslant 1$) as a function of θ are essentially similar to those of S1, S2, or S3. However, the lamellar phase contains many defects for longer copolymer chains. According to the SANS experiments,[56] the intermediate-segregation regime was identified as $\chi N_{AB}\approx 5-29$. Hence, S4 and S5 belong to the strong-segregation regime, whereas S6 (=S3) belongs to the intermediate-segregation regime. In the strong-segregation regime, the defects are hardly eliminated once they are created. The (inverse) characteristic length $\langle k\rangle$ is plotted as a function of θ for S4, S5, and S6 in Fig. 9 as before. The typical length scale is smaller for systems containing shorter copolymer chains. This means that the copolymer length dominates the overall structure.

For $\alpha=1$, Janert and Schick predicted a three-phase region at which the symmetric lamellar phase coexists with the A- and B-rich phases for large values of χN_A.[18] However, we have not observed this three-phase coexistence for $\alpha=1$ in our simulation. This is because the energy difference between the homogeneous lamellar phase and the three-phase coexisting state is too small to detect within our numerical accuracy.

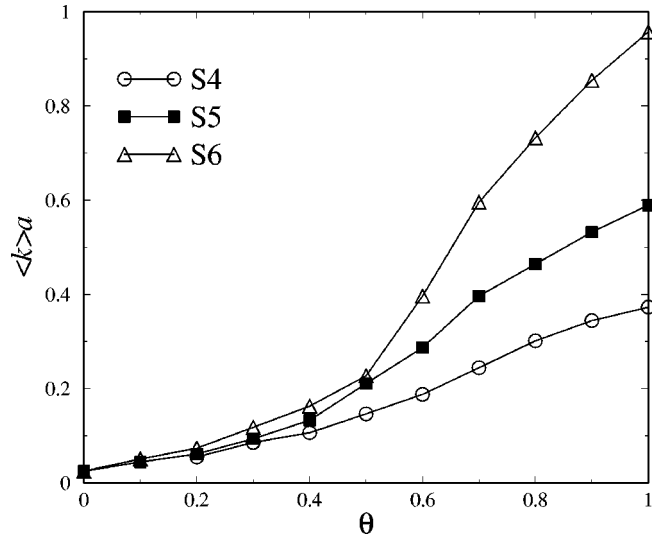

FIG. 9. The inverse characteristic length as a function of θ for systems 4, 5, and 6 in Table II which have the same homopolymer length but different copolymer length.

C. $\alpha>1$

We now show some results for the case of $\alpha>1$. As described in Sec. II, the Lifshitz point is preempted by the tricritical point beyond which there is a region of three-phase coexistence between A-rich, B-rich, and disordered phases[8] (see Fig. 3). The typical obtained patterns for system 7 (S7) and system 8 (S8) are depicted in Figs. 10 and 11, respectively. Also see Table III. The difference between these two systems is the value of Flory–Huggins interaction parameter χ. Compared to the case of $\alpha<1$, the patterns in these cases exhibit completely different sequences and the microphase separated bicontinuous structure does not appear. For intermediate θ ($\theta=0.3$, 0.5, and 0.7 in Fig. 10), the system is

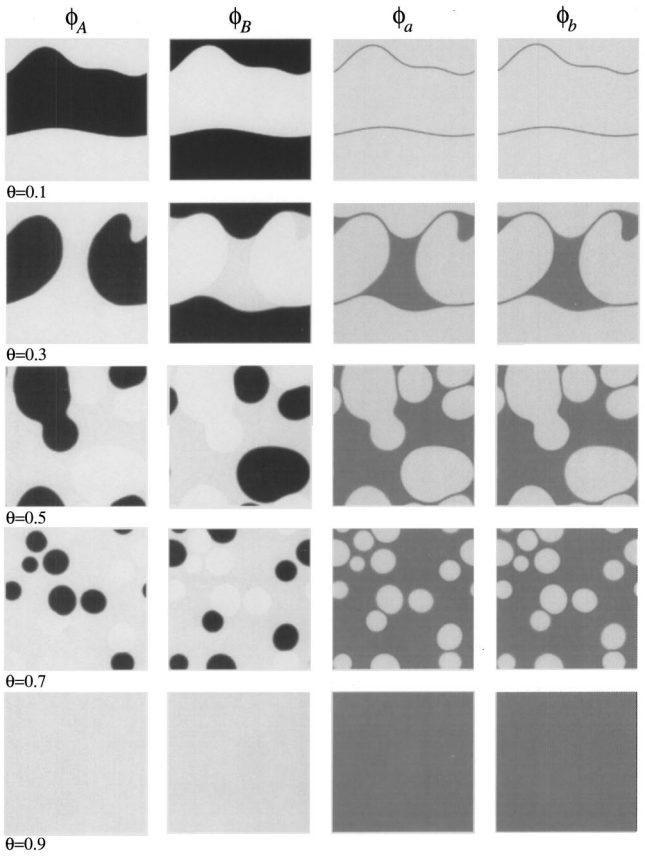

FIG. 10. Final patterns of system 7 in Table III. Notations are the same as those given in Fig. 4.

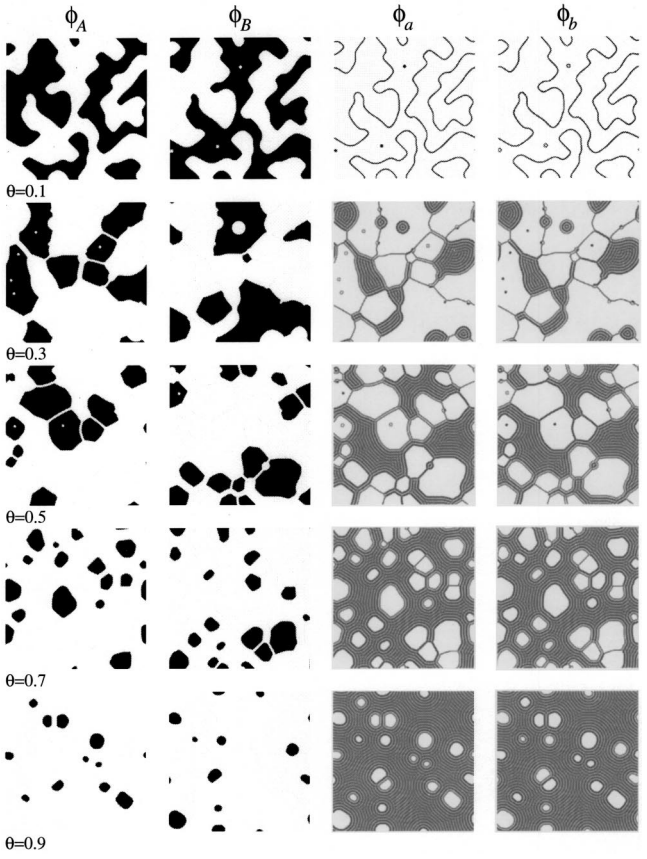

FIG. 11. Final patterns of system 8 in Table III. Notations are the same as those given in Fig. 4.

now in three-phase coexistence between A-rich, B-rich, and block copolymer rich phases, although the copolymer region is not microphase separated. For large θ ($\theta=0.9$ in Fig. 10), the homogeneous disordered phase is obtained. Notice that $\chi N_{AB}=8$ in S7 is smaller than $(\chi N_{AB})_{\mathrm{MST}}\approx 10.5$. These behaviors are consistent with the predicted phase diagram given in Fig. 3.

By increasing χ, the disordered AB copolymer region starts to microphase separate, and the system is in another three-phase coexistence between A-rich, B-rich, and lamellar phases. This situation can be observed for the intermediate θ in Fig. 11. It is interesting to note that the lamellar structure aligns parallel to the interface between other homogeneous phases, and the shape of domain is polygonal.

D. 3D case ($\alpha \leqslant 1$)

Here, we present some preliminary results from 3D simulations. Figure 12 shows typical configurations obtained from S2 for different θ. Shown is configuration of Δ in gray scale where values -1 and 1 correspond to white and black, respectively.

To characterize the geometrical properties of the surfaces, we measured various area averaged curvatures. So far, several methods have been proposed for the curvature determination of the bicontinuous structure.[57–59] For the surface defined implicitly by

$$\Sigma(x,y,z)=0, \tag{4.4}$$

we use here convenient expressions for the mean and Gaussian curvatures[60]

$$H=\frac{1}{2\Upsilon^3}[\Sigma_{xx}(\Sigma_y^2+\Sigma_z^2)-2\Sigma_x\Sigma_y\Sigma_{xy}+\mathrm{perm}], \tag{4.5}$$

$$K=\frac{1}{\Upsilon^4}[\Sigma_{xx}\Sigma_{yy}\Sigma_z^2-\Sigma_{xy}^2\Sigma_z^2+2\Sigma_{xz}\Sigma_x(\Sigma_y\Sigma_{yz}-\Sigma_z\Sigma_{yy}) + \mathrm{perm}]. \tag{4.6}$$

Here

$$\Upsilon=|\nabla\Sigma|, \tag{4.7}$$

and $\Sigma_i=\partial\Sigma/\partial r_i$, where $\mathbf{r}=(x,y,z)$, and "perm" indicates that two additional permutations of each term should be considered, i.e., one where $(x,y,z)\rightarrow(z,x,y)$ and another with $(x,y,z)\rightarrow(y,z,x)$.

The results for the average mean curvature squared $\langle H^2\rangle$, and for the average Gaussian curvature $\langle K\rangle$ for S1, S2, and S3 in Table I are shown as a function of θ in Fig. 13. Average over four different equilibrium configurations has been taken for each data point. The average mean curvature $\langle H\rangle$ vanishes due to the symmetry of the system. We see that the Gaussian curvature is negative, corresponding to a surface which is dominated by saddle-shaped configurations. For small θ, both $\langle H^2\rangle$ and $\langle K\rangle$ are small, corresponding to the macrophase separated structure in the symmetric system. For large θ, on the other hand, the system is dominated by the lamellar structure, and both curvatures take small values. It is interesting to note that there exist maximum and minimum of $\langle H^2\rangle$ and $\langle K\rangle$, respectively. Although it was difficult to distinguish between the three systems clearly in this analysis, we can at least say that the value of θ which gives the maximum of $\langle H^2\rangle$ or the minimum of $\langle K\rangle$ is smaller for smaller α as in S1.

E. Periodic initial conditions

Since it is probable that the patterns obtained so far may correspond to metastable equilibrium, one should also pay attention to the existence of equilibrium phases with LRO. To check this point, we performed the same numerical cal-

TABLE III. Characterization of the symmetric polymeric ternary systems for the same χN_A and α case ($\alpha>1$).

System	$N_A=N_B$	N_{AB}	α	χ	$\chi N_A=\chi N_B$	χN_{AB}	$(\theta_{\mathrm{TCP}},(\chi N_A)_{\mathrm{TCP}})$
system 7 (S7)	8	4	2	2	16	8	(4/5, 10)
system 8 (S8)	8	4	2	4	32	16	(4/5, 10)

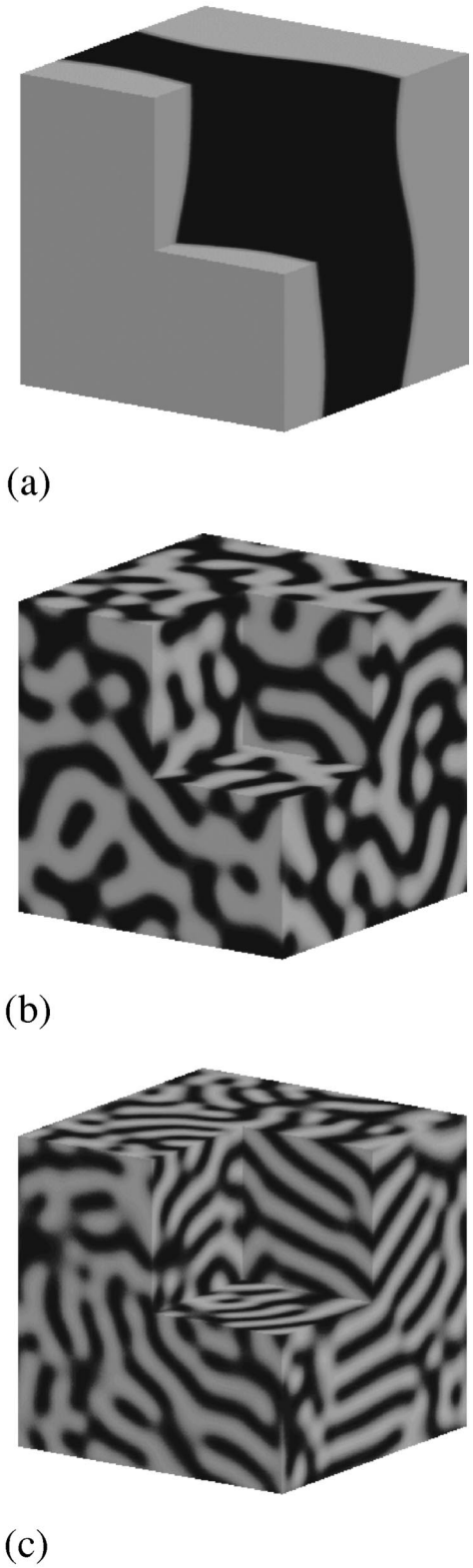

FIG. 12. Typical 3D final configuration for (a) $\theta=0.1$; (b) $\theta=0.6$; (c) $\theta=0.9$ of system 2. Shown is configuration of Δ in gray scale where values -1 and 1 correspond to white and black, respectively.

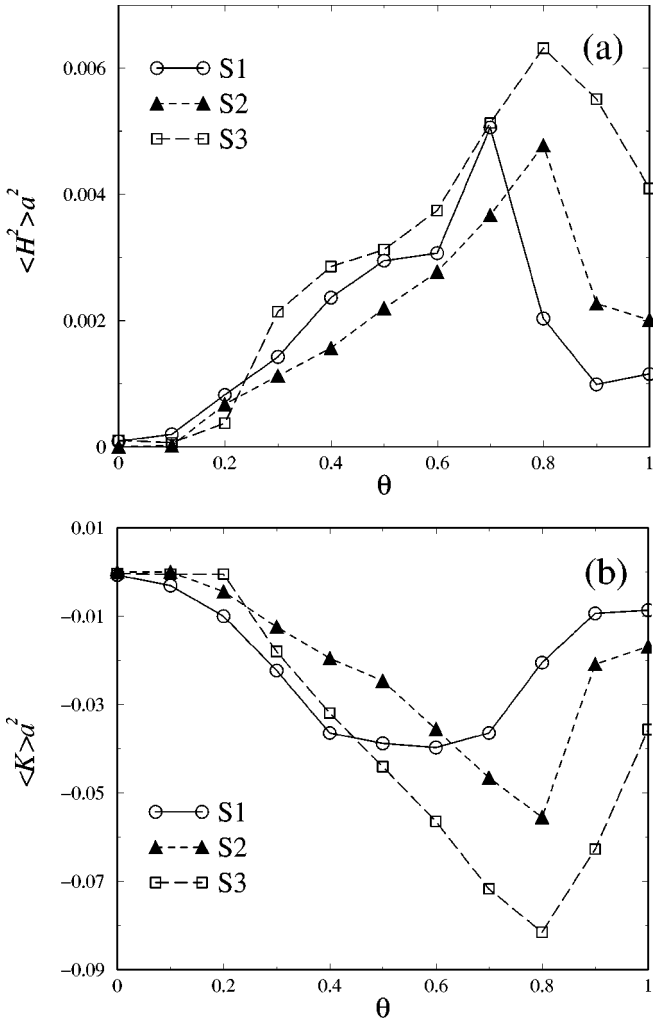

FIG. 13. (a) Average mean curvature squared $\langle H^2\rangle$ and (b) average Gaussian curvature squared $\langle K\rangle$ for systems 1, 2, and 3 in Table I which have the same copolymer length but different homopolymer length.

culations starting with the assumed 1D periodic potential fields and generated artificial lamellar structures. The parameters used in this case are listed in Table IV. Four different systems are considered as given from system 9 (S9) to system 12 (S12). Notice that $\alpha>1$ in S12. We then obtained the fully equilibrated lamellar phase by minimizing the free energy F_{m} in (3.10) with respect to the lamellar spacing.[61,62] The resulting free energy F_{m} is shown as a function of θ in Fig. 14(a). In Fig. 14(b), we plotted the deviation of the free energy from the tangent at $\theta=0.05$ for each curve in order to magnify its curvature. By carefully examining Fig. 14(b), we find that there are three distinct regions for each curve; region 1 (R1) where the profile is flat, region 2 (R2) where the curvature of the profile, $\partial^2 F_{\mathrm{m}}/\partial\theta^2$, is negative, and region 3 (R3) where the curvature is positive. These different regions are indicated in Fig. 14(b) for S12. One should note that only R3 is locally stable.

Physically speaking, the loss of configurational entropy of the homopolymer confined between the monolayers causes an attraction, while its translational entropy produces a repulsion. From the curvature of the free energy, we can discuss the effective interactions between the copolymer monolayers. The flat part of the free energy in R1 indicates that the local stability of the lamellar phase is marginal. In this region, arbitrary number of phases with different θ can coexist without any free-energy cost. This means that the

TABLE IV. Characterization of the symmetric polymeric ternary systems starting with 1D periodic initial conditions. * is the value for the tricritical point.

System	$N_A=N_B$	N_{AB}	α	χ	$\chi N_A=\chi N_B$	χN_{AB}	$(\theta_L,(\chi N_A)_L)$
system 9 (S9)	20	80	0.25	0.2	4	16	(1/9, 9/4)
system 10 (S10)	40	80	0.5	0.2	8	16	(1/3, 3)
system 11 (S11)	80	80	1	0.2	16	16	(2/3, 6)
system 12 (S12)	160	80	2	0.2	32	16	(4/5,10)*

copolymer monolayers do not interact with each other, and any separation distance between the monolayers within the corresponding range is allowed. Similar behavior has been predicted for a highly swollen lamellar phase in binary blends.[63,64]

For a certain region of small θ, we also find that ϕ_{AB} in the bulk region is independent of θ (≈ 0.01 for all the systems in Table IV) in R1. This value of ϕ_{AB} should coincide with the value of θ at which the lamellar periodicity diverges (unbinding transition)[17,18] and the free-energy curve is smoothly connected to that of two-phase state. Since we are considering the intermediate-segregation regime ($\chi N_{AB}=16$), $\theta \approx 0.01$ is much smaller than the Lifshitz volume fraction θ_L. We also point out that R1 is larger for relatively shorter copolymer chain. This is consistent with the result in Fig. 8, where the typical length scale increases for larger α.

Negative curvature in R2 results from the attractive interactions between the monolayers.[63,64] In this region, the lamellar phases in R1, R2 and a part of R3 are thermodynamically unstable, and macrophase separation into the lamellar, *A*-rich and *B*-rich phases (determined by a common tangent construction) should take place.[8,17,18] This unstable region hardly exists for S9 and S10, whereas it is remarkable for S12. This fact is consistent with the occurence of the three-phase coexistence shown in Fig. 11. Notice that the attractive interaction between the monolayers is present in the patterns of Fig. 5.

Similar to our work, Thompson and Matsen calculated the effective interactions between the monolayers by using the Fourier-space SCFT.[28] From the condition that the attraction becomes sufficiently small, they concluded that there is an optimum value of $\alpha \approx 0.8$ in order to emulsify the homopolymers. They further insist that emulsification efficiency is enhanced by introducing the copolymer polydispersity.[29]

V. SUMMARY AND CONCLUSION

In this paper, we have investigated the real-space structure of ternary blends of *A* and *B* homopolymers and symmetric *AB* diblock copolymer using an extended lattice (real-space) SCFT by means of numerical calculations. We restricted ourselves to the symmetric case where (i) both *A* and *B* homopolymers have the same length; (ii) the *AB* block copolymer is symmetric; (iii) the average volume fractions of *A* and *B* homopolymers are equal. We performed a systematic study to see how the copolymer fraction θ and the relative chain lengths $\alpha=N_A/N_{AB}$ affect the microphase separated structure. Starting with randomly generated initial potential fields, i.e., without assuming any symmetry of the

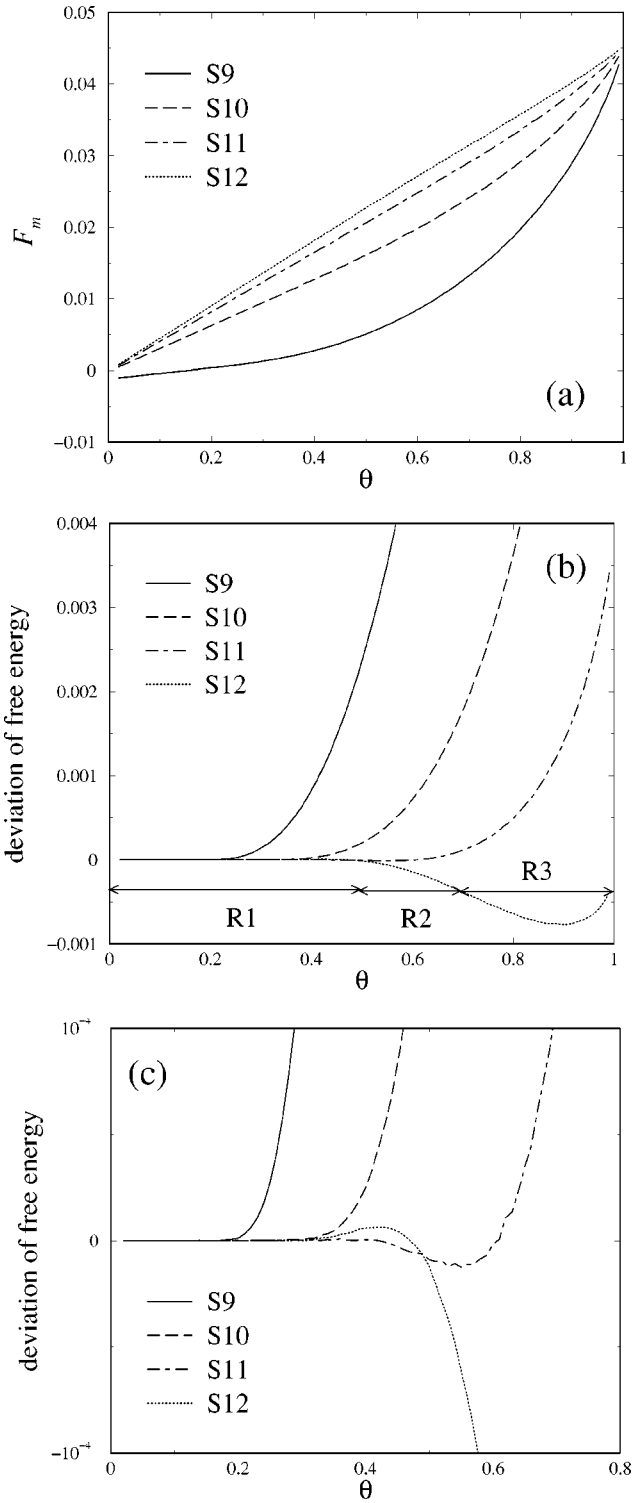

FIG. 14. (a) The free energy F_m as a function of θ for four different systems, and (b) its deviation from the tangent at $\theta=0.05$. (c) is the same plot with (b) magnified in the vertical axis.

mesophase *a priori*, we obtained various bicontinuous structures for $\alpha \leqslant 1$. For the fixed copolymer length, the typical length scale of the microphase separated structure becomes smaller for relatively shorter homopolymer chains (small α). This means that the homopolymers becomes more efficient to swell the microphase separated structure for longer homopolymer chains (large α). Some preliminary results of 3D simulations indicate that the average Gaussian curvature is negative corresponding to a surface which is dominated by saddle-shaped configurations. The bicontinuous patterns obtained for $\alpha \leqslant 1$ resemble the TEM images of PME found experimentally by Bates *et al.* Our result with random initial conditions shows, at least in the static sense, that PME with random configuration of interfaces results from microphase separation as metastable equilibrium.

The situation is different for $\alpha > 1$. In this case, the Lifshitz point is preempted by the tricritical point within the mean-field theory, and the three-phase coexistence between either the disorder, *A*-rich and *B*-rich phases or between the lamellar, *A*-rich and *B*-rich phases occurs. Here, the block copolymer rich phase can either be disordered or micro phase separated into the lamellar structure depending on the strength of the interaction parameter.

Since the obtained bicontinuous structures may correspond to metastable equilibrium, we have also performed the same numerical calculation starting from the initial potential fields with an imposed lamellar symmetry. Detailed free-energy analysis revealed that there is a region where the stability of the lamellar phase is marginal. This means that the copolymer monolayers do not interact each other in the corresponding region.

We finally comment that the metastable irregular defect structures obtained in 2D or 3D cases are due to the initially prepared random potential fields. In order to avoid such irregularities in real-space mean-field calculations, one can apply various tricks, such as by adding noise, adding external fields, or using a more realistic dynamics.[35] These methods will be included in our future calculations especially for 3D case.

Further developments of the present study, such as, asymmetric ternary system (asymmetry in α_A and α_B, asymmetry in $\overline{\phi}_A$ and $\overline{\phi}_B$, asymmetry in the block copolymer, etc.), homopolymer/copolymer binary system,[63,64] copolymer/copolymer binary system,[65,66] or different copolymer structure (e.g., *ABC* triblock copolymer[67]) are in progress.

ACKNOWLEDGMENTS

This work is supported by the Ministry of Education, Science and Culture, Japan (Grant-in-Aid for Scientific Research No. 09740318). S.K. thanks the Ministry of Education, Science and Culture, Japan for providing financial support during his visit to Weizmann Institute of Science, Israel. Support from the exchange program between the Japan Society for the Promotion of Science (JSPS) and the Israel Ministry of Science and Technology is also gratefully acknowledged. H.K. acknowledges the support from the Ministry of Education, Science and Culture, Japan (Grant-in-Aid for Scientific Research No. 13554001). We thank T. Kawakatsu, D. Andelman, and H. Orland for useful discussions.

APPENDIX A: EXTENDED LATTICE FORMULATION OF SCFT

In this Appendix, we give the detailed formulation of the extended lattice SCFT for the completeness of the present paper. All of the self-consistent equations in Sec. III B are derived here.

Some of the notations are repeated first. We denote the type of molecule by i, and the type of segment by J and K. Segments in a chain are indexed by $N'=1,2,\ldots,N_i$, where N_i is the polymerization index of the ith molecule. The molecules of type i are indexed by $p=1,2,\ldots,n_i$, where n_i is the total number of ith molecule.

We start to write the total Hamiltonian of the system as

$$\hat{\mathcal{H}}(\Gamma)=\hat{\mathcal{H}}_0(\Gamma)+\hat{\mathcal{W}}(\Gamma), \tag{A1}$$

where $\Gamma \equiv \{\mathbf{n}_{p,N'}^{(i)}\}$ represents the configuration space. The first term is the ideal Hamiltonian describing independent polymer chains represented as random walks, and is given by

$$\exp[-\hat{\mathcal{H}}_0(\Gamma)]=\prod_i \prod_{p=1}^{n_i} \prod_{N'=1}^{N_i-1} \delta[|\mathbf{n}_{p,N'+1}^{(i)}-\mathbf{n}_{p,N'}^{(i)}|,1], \tag{A2}$$

where the Kronecker delta function is defined in Sec. III B. Next, the interaction Hamiltonian $\hat{\mathcal{W}}(\Gamma)$ is assumed to to be written as a density functional form $\hat{\mathcal{W}}(\Gamma) = \mathcal{W}[\{\hat{\phi}_J(\mathbf{n};\Gamma)\}]$, where

$$\hat{\phi}_J(\mathbf{n};\Gamma)=\sum_i \sum_{p=1}^{n_i} \sum_{N'=1}^{N_i} \delta[\mathbf{n},\mathbf{n}_{p,N'}^{(i)}]\delta[J,f_i(N')] \tag{A3}$$

is the microscopic representation of the segment density field. The "type function" $f_i(N')$ is also introduced in Sec. III B. The functional form of $\mathcal{W}$ is given by

$$\mathcal{W}[\{\phi_J(\mathbf{n})\}]=\frac{1}{2}\sum_{\mathbf{n}} \sum_{J,K} \chi_{JK}\,\phi_J(\mathbf{n})\langle\langle\phi_K(\mathbf{n})\rangle\rangle. \tag{A4}$$

In the above, χ_{JK} is the Flory–Huggins parameter between J and K segments, and $\langle\langle X(\mathbf{n})\rangle\rangle$ denotes the average of $X(\mathbf{n})$ over the nearest-neighbor lattice sites

$$\langle\langle X(\mathbf{n})\rangle\rangle=\frac{1}{z}\sum_{\mathbf{n}'} \delta[|\mathbf{n}-\mathbf{n}'|,1]X(\mathbf{n}'), \tag{A5}$$

where z is the number of the nearest-neighbor sites ($z=6$ for a cubic lattice). At the end of this Appendix, we will extend this definition.

Under the incompressibility condition

$$\sum_J \phi_J(\mathbf{n})=1, \tag{A6}$$

the partition function is calculated by

$$\mathcal{Z}=\frac{1}{\Pi_i n_i!}\sum_{\{\Gamma\}}\exp[-\hat{\mathcal{H}}(\Gamma)]$$
$$=\int\mathcal{D}[\phi_J(\mathbf{n})]\int\mathcal{D}[U_J(\mathbf{n})]\times\exp\Bigg[\log\mathcal{Z}_e[U_J]-\mathcal{W}[\phi_J]+\sum_{\mathbf{n}}\sum_J U_J(\mathbf{n})\phi_J(\mathbf{n})\Bigg]\times\exp\Bigg[-\sum_{\mathbf{n}}u(\mathbf{n})\Bigg(\sum_J\phi_J(\mathbf{n})-1\Bigg)\Bigg]. \quad (A7)$$

Here, $u(\mathbf{n})$ is a Lagrange multiplier to incorporate the constraint of the incompressibility condition (A6), and $\mathcal{Z}_e[U_J]$ is a partition function of the chains interacting with the external potential field $\{U_J(\mathbf{n})\}$, i.e.,

$$\mathcal{Z}_e[U_J]=\frac{1}{\Pi_i n_i!}\sum_{\{\Gamma\}}\exp[-\hat{\mathcal{H}}_0(\Gamma)-\hat{\mathcal{W}}'(\Gamma)], \quad (A8)$$

with

$$\hat{\mathcal{W}}'(\Gamma)=\sum_J\sum_i\sum_{p=1}^{n_i}\sum_{N'=1}^{N_i}\delta[J,f_i(N')]U_J(\mathbf{n}^{(i)}_{p,N'}). \quad (A9)$$

From (A7) we obtain the mean-field free energy as

$$F[\phi_J,U_J]=-\log\mathcal{Z}_e[U_J]+\mathcal{W}[\phi_J]-\sum_{\mathbf{n}}\sum_J U_J(\mathbf{n})\phi_J(\mathbf{n}), \quad (A10)$$

together with the saddle-point conditions

$$U_J(\mathbf{n})=u(\mathbf{n})+\sum_K\chi_{JK}\langle\langle\phi_K(\mathbf{n})\rangle\rangle, \quad (A11)$$

and

$$\phi_J(\mathbf{n})=-\frac{1}{\mathcal{Z}_e}\frac{\delta\mathcal{Z}_e[U_J]}{\delta U_J(\mathbf{n})}. \quad (A12)$$

Inserting (A2) and (A9) into (A8), we get

$$\mathcal{Z}_e[U_J]=\prod_i\frac{1}{n_i!}(\mathcal{Z}_i[U_J])^{n_i}, \quad (A13)$$

where $\mathcal{Z}_i[U_J]$ is the single chain partition function

$$\mathcal{Z}_i[U_J]=\sum_{\{\Gamma_i\}}\Bigg\{\prod_{N'=1}^{N_i-1}\delta[|\mathbf{n}^{(i)}_{N'+1}-\mathbf{n}^{(i)}_{N'}|,1]\Bigg\}\times\exp\Bigg[-\sum_J\sum_{N''=1}^{N_i}\delta[J,f_i(N'')]U_J(\mathbf{n}^{(i)}_{N'})\Bigg], \quad (A14)$$

with $\Gamma_i\equiv(\mathbf{n}^{(i)}_{N_0}\cdots\mathbf{n}^{(i)}_{N_1})$ representing the configuration space of single ith molecule. By substituting (A13) and (A14) into (A12), $\phi_J(\mathbf{n})$ can be expressed as

$$\phi_J(\mathbf{n})=\sum_i\sum_{N'=1}^{N_i}\delta[J,f_i(N')]\phi_{i,N'}(\mathbf{n}), \quad (A15)$$

where the single segment distribution is

$$\phi_{i,N'}(\mathbf{n})=\frac{n_i}{\mathcal{Z}_i}\sum_{\{\Gamma_i\}}\delta[\mathbf{n},\mathbf{n}^{(i)}_{N'}]\Bigg\{\prod_{N''=1}^{N_i-1}\delta[|\mathbf{n}^{(i)}_{N''+1}-\mathbf{n}^{(i)}_{N''}|,1]\Bigg\}\times\exp\Bigg[-\sum_J\sum_{N'''=1}^{N_i}\delta[J,f_i(N''')]U_J(\mathbf{n}^{(i)}_{N'''})\Bigg]. \quad (A16)$$

Up to now, the problem has been reduced to that of a single chain statistics under the external potential $U_J(\mathbf{n})$ (A11) with the incompressibility condition (A6). This problem should be solved in a self-consistent manner. In the ith chain, let us define the following two-point correlation function for the positions of the segments $N'=N_0$ and N_1:

$$Q_i(\mathbf{n}_0,N_0;\mathbf{n}_1,N_1)=\frac{1}{\Omega z^{|N_1-N_0|}}\sum_{\{\Gamma_i\}}\Bigg\{\prod_{N'=N_0}^{N_1-1}\delta[|\mathbf{n}^{(i)}_{N'+1}-\mathbf{n}^{(i)}_{N'}|,1]\Bigg\}\times\exp\Bigg[-\sum_J\sum_{N''=N_0}^{N_1}\delta[J,f_i(N'')]U_J(\mathbf{n}^{(i)}_{N''})\Bigg]\times\delta[\mathbf{n}_0,\mathbf{n}^{(i)}_{N_0}]\ \delta[\mathbf{n}_1,\mathbf{n}^{(i)}_{N_1}]. \quad (A17)$$

Notice that Ωz^{N-1} is the partition function of a single ideal chain of polymerization index N. We next define the forward and backward end-segment statistical weights as

$$G_i(\mathbf{n},N')=\Omega\sum_{\mathbf{n}_0}Q_i(\mathbf{n}_0,1;\mathbf{n},N'), \quad (A18)$$

and

$$G_i^\dagger(\mathbf{n},N')=\Omega\sum_{\mathbf{n}_1}Q_i(\mathbf{n},N';\mathbf{n}_1,N_i), \quad (A19)$$

respectively. The single segment distribution $\phi_{i,N'}(\mathbf{n})$ in (A16) can be rewritten in terms of the end-segment statistical weights as

$$\phi_{i,N'}(\mathbf{n})=\frac{n_iG_i(\mathbf{n},N')G_i^\dagger(\mathbf{n},N')}{\exp[-U_{f_i(N')}(\mathbf{n})]\Sigma_{\mathbf{n}'}G_i(\mathbf{n}',N_i)}. \quad (A20)$$

It is straightforward to see that end-segment statistical weights satisfy the following recursive relations:

$$G_i(\mathbf{n},N')=\exp[-U_{f_i(N')}(\mathbf{n})]\langle\langle G_i(\mathbf{n}',N'-1)\rangle\rangle, \quad (A21)$$

$$G_i^\dagger(\mathbf{n},N')=\exp[-U_{f_i(N')}(\mathbf{n})]\langle\langle G_i^\dagger(\mathbf{n}',N'+1)\rangle\rangle, \quad (A22)$$

together with the initial conditions

$$G_i(\mathbf{n},1)=\exp[-U_{f_i(1)}(\mathbf{n})], \quad (A23)$$

$$G_i^\dagger(\mathbf{n},N_i)=\exp[-U_{f_i(N_i)}(\mathbf{n})]. \quad (A24)$$

By comparing from (A17) to (A19) with (A14), we see that the single chain partition function can be rewritten as

$$\mathcal{Z}_i[U_J]=z^{N_i}\sum_{\mathbf{n}} G_i(\mathbf{n},N_i)=z^{N_i}\sum_{\mathbf{n}} G_i^{\dagger}(\mathbf{n},1). \tag{A25}$$

The unmixed pure system is taken as a reference system in which all the segment interactions are switched off. The free energy of such a reference system is

$$F_0=-\log \mathcal{Z}_0, \tag{A26}$$

with the partition function

$$\mathcal{Z}_0=\prod_i \frac{(\Omega_i z^{N_i})^{n_i}}{n_i!}. \tag{A27}$$

Here, $\Omega_i=n_iN_i$ is the total number of lattice sites occupied by the pure system consisting of the ith molecule. From (A10) and (A26), we finally calculate the mixed free energy F_{m} with respect to the reference system as

$$\begin{aligned}F_{\mathrm{m}}[\phi_J,U_J]&=F[\phi_J,U_J]-F_0\\&=\sum_i n_i\log\frac{n_iN_i}{\Sigma_{\mathbf{n}}G_i(\mathbf{n},N_i)}\\&\quad+\frac{1}{2}\sum_{\mathbf{n}}\sum_{J,K}\chi_{JK}\phi_J(\mathbf{n})\langle\langle\phi_K(\mathbf{n})\rangle\rangle\\&\quad-\sum_{\mathbf{n}}\sum_J U_J(\mathbf{n})\phi_J(\mathbf{n}).\end{aligned} \tag{A28}$$

We now extend the present lattice SCFT formulation in order to avoid the geometric constraints associated with a lattice. For this purpose, we redefine the ideal Hamiltonian in (A2) as

$$\begin{aligned}\exp[-\hat{\mathcal{H}}_0(\Gamma)]=\prod_i\prod_{p=1}^{n_i}\prod_{N'=1}^{N_i-1}\Big(&\delta[|\mathbf{n}^{(i)}_{p,N'+1}-\mathbf{n}^{(i)}_{p,N'}|^2,1]\\&+\frac{1}{2}\delta[|\mathbf{n}^{(i)}_{p,N'+1}-\mathbf{n}^{(i)}_{p,N'}|^2,2]\\&+\frac{1}{6}\delta[|\mathbf{n}^{(i)}_{p,N'+1}-\mathbf{n}^{(i)}_{p,N'}|^2,3]\Big).\end{aligned} \tag{A29}$$

This is an important extension in our work to deal with isotropic structures. According to (A29), the definition of the neighborhood average should be modified as[51]

$$\begin{aligned}\langle\langle X(\mathbf{n})\rangle\rangle=\sum_{\mathbf{n}'}\Big[&\frac{6}{80}\delta[|\mathbf{n}-\mathbf{n}'|^2,1]+\frac{3}{80}\delta[|\mathbf{n}-\mathbf{n}'|^2,2]\\&+\frac{1}{80}\delta[|\mathbf{n}-\mathbf{n}'|^2,3]\Big]X(\mathbf{n}'),\end{aligned} \tag{A30}$$

which is used in our simulations.

Equations (A6), (A11), (A15), (A20), (A21), (A22), (A23), (A24), and (A30) form a set of self-consistent equations given in Sec. III B.

We finally comment that a different definition of the ideal Hamiltonian gives rise to different Kuhn's statistical segment length b_{K}. For (A5), we have $b_{\mathrm{K}}=a$, whereas for (A29), we have $b_{\mathrm{K}}=(33/20)a$.

APPENDIX B: ITERATION SCHEME

Here, we describe the iteration scheme proposed by Hasegawa to solve the set of self-consistent equations.[30] A similar Picard-type iteration scheme has been used by others.[34,68]

The new estimates for $\{U_J(\mathbf{n})\}$ are calculated from the previous ones according to the following rule:

$$\begin{aligned}U_J^{(T+1)}(\mathbf{n})=U_J^{(T)}(\mathbf{n})&+c_1\Big[\sum_J\phi_J^{(T)}(\mathbf{n})-1\Big]\\&+c_2\Big[\frac{\Sigma_L(U_L^{(T)}(\mathbf{n})-\Sigma_M\chi_{LM}\langle\langle\phi_M^{(T)}(\mathbf{n})\rangle\rangle)}{\Sigma_L 1}\\&-\Big(U_J^{(T)}(\mathbf{n})-\sum_K\chi_{JK}\langle\langle\phi_K^{(T)}(\mathbf{n})\rangle\rangle\Big)\Big],\end{aligned} \tag{B1}$$

where c_1 and c_2 are positive constants and $T=0,1,\ldots$. This iteration scheme is continued until the quantity ϵ defined by

$$\begin{aligned}\epsilon=\sum_{\mathbf{n}}\Big[&\Big|\sum_J\phi_J^{(T)}(\mathbf{n})-1\Big|^2\\&+\sum_J\Big|\frac{\Sigma_L(U_L^{(T)}(\mathbf{n})-\Sigma_M\chi_{LM}\langle\langle\phi_M^{(T)}(\mathbf{n})\rangle\rangle)}{\Sigma_L 1}\\&-\Big(U_J^{(T)}(\mathbf{n})-\sum_K\chi_{JK}\langle\langle\phi_K^{(T)}(\mathbf{n})\rangle\rangle\Big)\Big|^2\Big],\end{aligned} \tag{B2}$$

becomes less than 10^{-6}. The time step required for the convergence strongly depends on the choice of c_1 and c_2.

[1] G. Gompper and M. Schick, *Self-Assembling Amphiphilic Systems* (Academic, London, 1994).
[2] *Micelles, Membranes, Microemulsions, and Monolayers*, edited by W. M. Gelbart, A. Ben-Shaul, and D. Roux (Springer, New York, 1994).
[3] W. Jahn and R. Strey, J. Phys. Chem. **92**, 2294 (1988).
[4] R.-J. Roe and D. Rigby, Adv. Polym. Sci. **82**, 103 (1987).
[5] I. W. Hamley, *The Physics of Block Copolymers* (Oxford University Press, Oxford, 1998).
[6] L. Leibler, Makromol. Chem., Rapid Commun. **2**, 393 (1981).
[7] L. Leibler, Macromolecules **15**, 1283 (1982).
[8] D. Broseta and G. H. Fredrickson, J. Chem. Phys. **93**, 2927 (1990).
[9] R. Holyst and M. Schick, J. Chem. Phys. **96**, 7728 (1992).
[10] J. Noolandi and K. M. Hong, Macromolecules **15**, 482 (1982).
[11] J. Noolandi and K. M. Hong, Macromolecules **17**, 1531 (1984).
[12] K. R. Shull and E. J. Kramer, Macromolecules **23**, 4769 (1990).
[13] K. R. Shull, E. J. Kramer, G. Hadziioannou, and W. Tang, Macromolecules **23**, 4780 (1990).
[14] H. K. Dai, E. J. Kramer, and K. R. Shull, Macromolecules **25**, 220 (1992).
[15] M. Banaszak and M. D. Whitmore, Macromolecules **25**, 249 (1992).
[16] R. Israels, D. Jasnow, A. C. Balazs, L. Guo, G. Krausch, J. Sokolov, and M. Rafailovich, J. Chem. Phys. **102**, 8149 (1995).
[17] P. K. Janert and M. Schick, Macromolecules **30**, 137 (1997).
[18] P. K. Janert and M. Schick, Macromolecules **30**, 3916 (1997).
[19] F. S. Bates, W. W. Maurer, P. M. Lipic, M. A. Hillmyer, K. Almdal, K. Mortensen, G. H. Fredrickson, and T. P. Lodge, Phys. Rev. Lett. **79**, 849 (1997).
[20] G. H. Fredrickson and F. S. Bates, J. Polym. Sci., Part B: Polym. Phys. **35**, 2775 (1997).
[21] M. A. Hillmyer, W. W. Maurer, T. P. Lodge, and F. S. Bates, J. Phys. Chem. B **103**, 4814 (1999).
[22] T. L. Morkved, B. R. Chapman, F. S. Bates, T. P. Lodge, P. Stepanek, and K. Almdal, Faraday Discuss. **112**, 335 (1999).
[23] H. S. Jeon, J. H. Lee, and N. P. Balsara, Phys. Rev. Lett. **79**, 3274 (1997).
[24] H. S. Jeon, J. H. Lee, N. P. Balsara, and M. C. Newstein, Macromolecules **31**, 3340 (1998).

[25] L. Kielhorn and M. Muthukumar, J. Chem. Phys. **107**, 5588 (1997).
[26] L. Kielhorn and M. Muthukumar, J. Chem. Phys. **110**, 4079 (1999).
[27] M. W. Matsen, J. Chem. Phys. **110**, 4658 (1999).
[28] R. B. Thompson and M. W. Matsen, J. Chem. Phys. **112**, 6863 (2000).
[29] R. B. Thompson and M. W. Matsen, Phys. Rev. Lett. **85**, 670 (2000).
[30] R. Hasegawa, thesis, Nagoya University (1997).
[31] S. Komura, H. Kodama, and K. Tamura, in *Slow Dynamics in Complex Systems*, edited by M. Tokuyama and I. Oppenheim (AIP, New York, 1999), pp. 188–189.
[32] H. Kodama and S. Komura, in *Statistical Physics*, edited by M. Tokuyama and H. E. Stanley (AIP, New York, 2000), pp. 247–249.
[33] H. Kodama, S. Komura, and K. Tamura, Europhys. Lett. **53**, 46 (2001).
[34] F. Drolet and G. H. Fredrickson, Phys. Rev. Lett. **83**, 4317 (1999).
[35] F. Drolet and G. H. Fredrickson, Macromolecules **34**, 5317 (2001).
[36] Y. Bohbot-Raviv and Z.-G. Wang, Phys. Rev. Lett. **85**, 3428 (2000).
[37] G. H. Fredrickson, V. Ganesan, and F. Drolet, Macromolecules **35**, 16 (2002).
[38] R. M. Hornreich, M. Luban, and S. Shtrikman, Phys. Rev. Lett. **35**, 1678 (1975).
[39] P. M. Chaikin and T. C. Lubensky, *Principles of Condensed Matter Physics* (Cambridge University Press, Oxford, 1995).
[40] M. Teubner and R. Strey, J. Chem. Phys. **87**, 3195 (1987).
[41] M. W. Matsen and M. Schick, Macromolecules **26**, 3878 (1993).
[42] S. F. Edwards, Proc. Phys. Soc. London **85**, 613 (1965).
[43] E. Helfand and Y. Tagami, J. Polym. Sci. [B] **9**, 741 (1971); J. Chem. Phys. **56**, 3592 (1971); **57**, 1812 (1972); **62**, 999 (1975).
[44] For a review, see F. Schmid, J. Phys.: Condens. Matter **10**, 8105 (1998).
[45] M. W. Matsen and M. Schick, Phys. Rev. Lett. **72**, 2660 (1994); Macromolecules **27**, 4014 (1994).
[46] M. W. Matsen and F. Bates, Macromolecules **29**, 1091 (1996).
[47] J. M. H. M. Scheutjens and G. J. Fleer, J. Phys. Chem. **83**, 1619 (1979).
[48] G. J. Fleer, M. A. Cohen Stuart, J. M. H. M. Scheutjens, T. Cosgrove, and B. Vincent, *Polymers at Interfaces* (Chapman & Hall, London, 1993).
[49] O. E. Evers, J. M. H. M. Scheutjens, and G. J. Fleer, Macromolecules **23**, 5221 (1990); J. Chem. Soc., Faraday Trans. **86**, 1333 (1990).
[50] B. A. C. van Vlimmeren, N. M. Maurits, A. V. Zvelindovsky, G. J. A. Sevink, and J. G. E. M. Fraaije, Macromolecules **32**, 646 (1999); J. G. E. M. Fraaije, B. A. C. van Vlimmeren, N. M. Maurits, M. Postma, O. A. Evers, C. Hoffmann, P. Altevogt, and G. Goldbeck-Wood, J. Chem. Phys. **106**, 4260 (1997); G. T. Pickett and A. C. Balazs, Macromol. Theory Simul. **7**, 249 (1998).
[51] A. Shinozaki and Y. Oono, Phys. Rev. E **48**, 2622 (1993).
[52] N. M. Maurits, J. G. E. M. Fraaije, P. Altevogt, and O. A. Evers, Comput. Theor. Polym. Sci. **6**, 1 (1996).
[53] J. G. E. M. Fraaije, J. Chem. Phys. **99**, 9202 (1993).
[54] L. Leibler, Macromolecules **13**, 1602 (1980).
[55] M. Kotlarchyk, S.-H. Chen, J. S. Huang, and M. W. Kim, Phys. Rev. Lett. **53**, 941 (1984).
[56] C. M. Papadakis, K. Almdal, K. Mortensen, and D. Posselt, Europhys. Lett. **36**, 289 (1996); J. Phys. II **7**, 1829 (1997).
[57] G. Gompper and M. Kraus, Phys. Rev. E **47**, 4301 (1993).
[58] H. Jinnai, T. Koga, Y. Nishikawa, T. Hashimoto, and S. T. Hyde, Phys. Rev. Lett. **78**, 2248 (1997); Y. Nishikawa, H. Jinnai, T. Koga, T. Hashimoto, and S. T. Hyde, Langmuir **14**, 1242 (1998).
[59] S.-H. Chen and S.-M. Choi, J. Appl. Crystallogr. **30**, 755 (1997); S.-M. Choi and S.-H. Chen, Prog. Colloid Polym. Sci. **106**, 14 (1997).
[60] S. A. Safran, *Statistical Thermodynamics of Surfaces, Interfaces, and Membranes* (Addison-Wesley, Reading, MA, 1994).
[61] J. Noolandi, A.-C. Shi, and P. Linse, Macromolecules **29**, 5907 (1996).
[62] M. Svensson, P. Alexandridis, and P. Linse, Macromolecules **32**, 637 (1999).
[63] M. W. Matsen, Phys. Rev. Lett. **74**, 4225 (1995).
[64] M. W. Matsen, Macromolecules **28**, 5765 (1995).
[65] M. W. Matsen, J. Chem. Phys. **103**, 3268 (1995).
[66] P. D. Olmsted and I. W. Hamley, Europhys. Lett. **45**, 83 (1999).
[67] G. H. Fredrickson and F. S. Bates, Eur. Phys. J. B **1**, 71 (1998).
[68] A.-C. Shi, J. Noolandi, and R. C. Desai, Macromolecules **29**, 6487 (1996); K. R. Shull, *ibid.* **26**, 2346 (1993).